# CHAPTER 5

# LIQUEFACTION EVALUATION USING SHAKE TABLE TEST

## 5.1 General

This chapter elucidate the effect of hydrocarbon contamination on the pore pressure behavior of Guwahati sand, the area lying in earthquake zone V and contains numerous oilfields nearby. Shake table tests were conducted to study the effect of degree of contamination in terms of crude oil content (ω), depth of contamination in terms of contamination depth ratio (β), defined as the ratio of contaminated depth to the total considered depth, and shaking history. The model setup, instrumentation and control for the test rig is described in detail. The liquefaction potential was evaluated in terms of normalized pore pressure ratio. Finally, the test results and summary of the observations are discussed.

## 5.2 Test Procedures and Conditions

### *5.2.1 Test Procedures*

This test was based on the assessment of excess pore fluid pressure at a particular depth/overburden pressure. In this test, two pore pressure transducers were embedded at certain depths into the sand contained in a test box. The base of the test box was attached to an actuator to liquefy the soil through base shaking by developing excess pore fluid pressure. In the present study the tests were carried out with following objectives:

1. To understand the change in excess pressure pressure-time histories in Guwahati sand and crude oil contaminated Guwahati sand.

2. To directly investigate the effect of crude oil contamination on the liquefaction potential of the Guwahati Sand.

*5.2.2 Test Conditions*

A series of 63 base shaking events were conducted to extensively study the effect of degree of crude oil contamination (ω%), contamination depth ratio (β) and shaking history on the cyclic pore pressure response of Guwahati Sand. The shaking table along with the model container was subjected to a displacement-controlled sinusoidal base shaking. As per the GSHAP model proposed by Bhatia et al. (1999), the area under consideration lies in the zone of 0.25g-0.35g PGA with 10% probability of exceedance in 50 years. Therefore, the entire study was conservatively conducted at peak ground acceleration (PGA) of 0.35g (Banerjee et al. 2017) which was supposed to be large enough to induce liquefaction. Table 5.1 shows the test matrix of the proposed study. Each test combination was subjected to three shaking events. The detailed schedule of these multiple shaking events has been summarized in Fig. 5.1. The intensity of input motion was kept same for all three shaking events; however, the duration of shaking was increased by twenty seconds for each subsequent shaking. The design intent of these multiple events is to investigate whether the same sand bed re-liquefies under the same base excitation but for a longer duration. The time interval between the two subsequent shaking events was established considering the time required for excess pore pressure to dissipate. Prior to first shaking event, the relative density of the sand bed for each test was kept uniform in the range of 40-43%. After each shake, the amount of densification is estimated by manually measuring the settlement of the top surface of the sand bed at four different locations.

**Table 5.1 Summary of shake table tests**

| Sample Type | Contamination depth ratio | Crude oil content (%) | Shaking event |
|---|---|---|---|
| Homogeneous | β = 0 | ω = 0 | Shake 1 |
| | | | Shake 2 |
| | | | Shake 3 |
| | β = 1 | ω = 2, 4, 6, 8, 10 | Shake 1 |
| | | | Shake 2 |
| | | | Shake 3 |
| Layered | β = 0.356 | ω = 2, 4, 6, 8, 10 | Shake 1 |
| | | | Shake 2 |
| | | | Shake 3 |
| | β = 0.55 | ω = 2, 4, 6, 8, 10 | Shake 1 |
| | | | Shake 2 |
| | | | Shake 3 |
| | β = 0.75 | ω = 2, 4, 6, 8, 10 | Shake 1 |
| | | | Shake 2 |
| | | | Shake 3 |

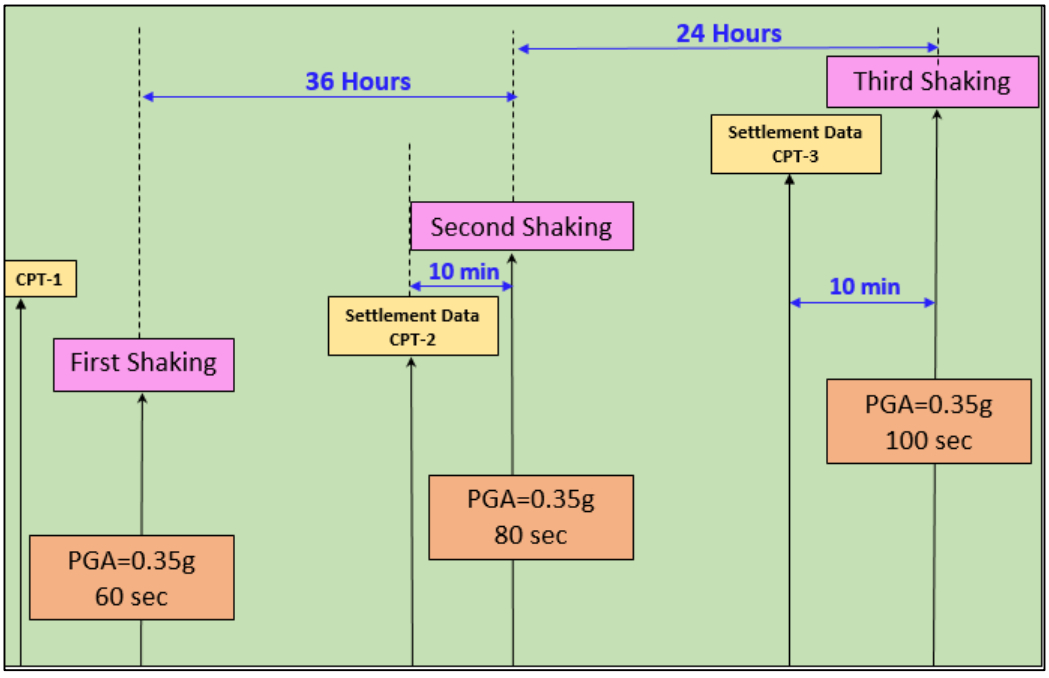


**Fig. 5.1 Schedule of multiple shaking events**

### 5.2.3 *Cone Penetration Test (CPT)*

The pre-shaking and post-shaking CPT tests were also conducted to determine the relative compactness of the sand along the model depth before and after each shaking. It involved raising and dropping a hammer to drive the cone on the lower shaft through the underlying sand layer. The detailed specifications of the Dynamic Cone Penetration Test (DCPT) set up used in the study is given in Fig. 5.2.

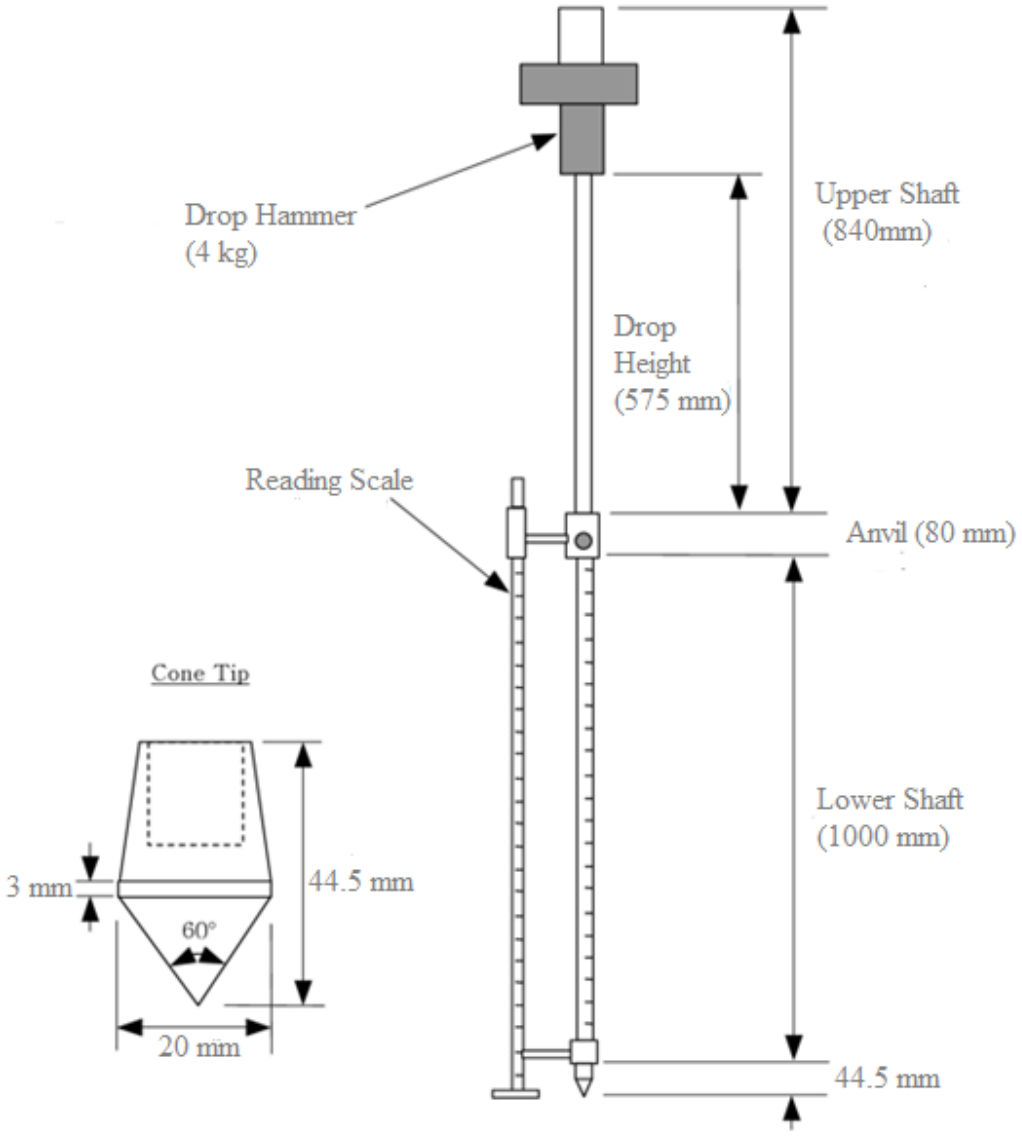


**Fig. 5.2 Specifications of DCPT unit**

The system consists of a drop hammer of 4 kg which is dropped from a height of 57.5 cm onto an anvil. The anvil is attached to a lower shaft which is equipped with a sharp cone at its bottom end. The tip angle of the cone is $60^0$ and its diameter is 2 cm. The impact of hammer on the anvil forces the cone to penetrate into the sand bed. The penetration is recorded with the help of a measuring scale behind the lower shaft. The arrangement for conducting CPT test inside the testing tank has been shown in Fig. 5.3. The penetration of the cone was recorded corresponding to each blow and is termed as DCP penetration index (DPI). It is expressed in mm/blow. Lower DPI indicates higher relative compactness and vice versa.

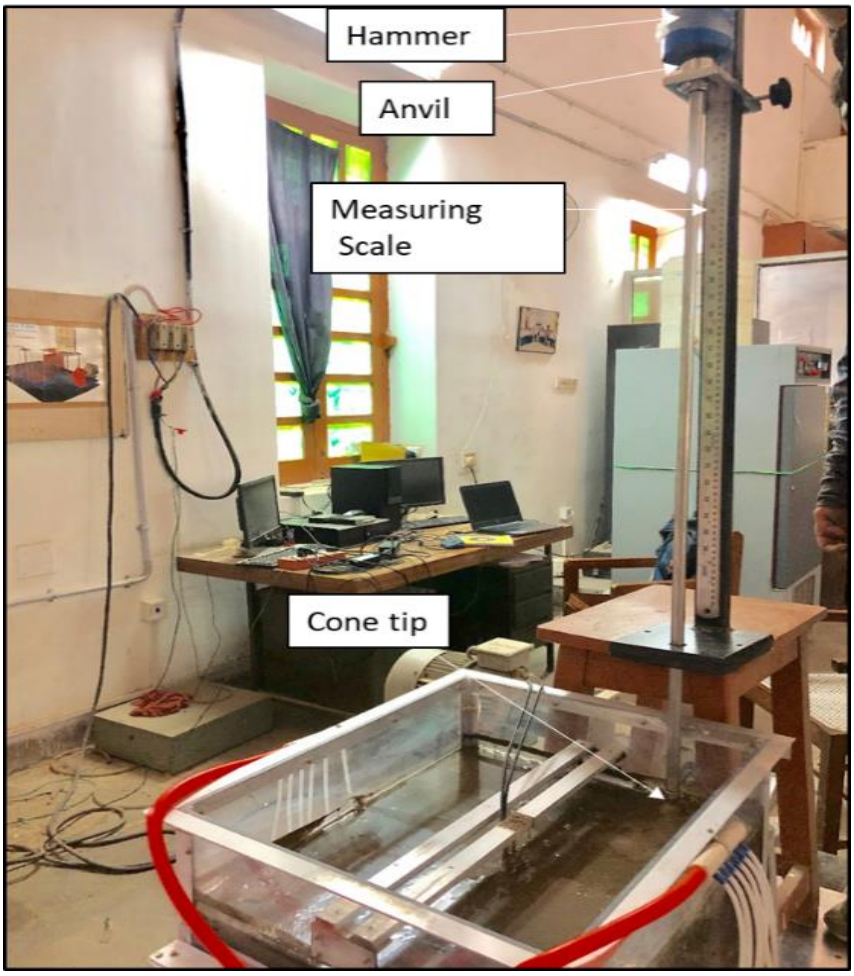


**Fig. 5.3 Arrangement for CPT test**

*5.2.4 Shake Table*

The model tests reported in this study were carried out on a uniaxial shaking table having a payload capacity of 0.2 tonne. The photographic view of shake table is shown in Fig 5.4 along with its specifications in Table 5.2. The size of the shaking platform was 1000 x 1000 mm which can be triggered with different frequencies ranging between 0 and 20 Hz and simulates the horizontal ground shaking effects.

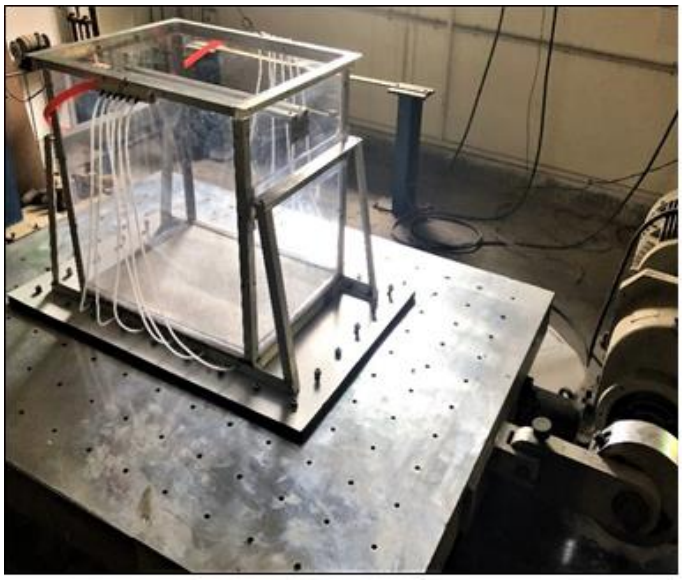

**Fig. 5.4 Photographic view of shake table**

**Table 5.2 Specifications of shake table**

| **Specifications** | |
|---|---|
| Motion | Horizontal (Uniaxial) |
| Maximum Pay Load | 200 Kgs |
| Top Table Size | 1500mm x 1200mm |
| Frequency Range | 0-20 Hz |
| Frequency Control | Within +/- 5% |
| Amplitude | +/- 50mm or total 100mm |
| Amplitude Resolution | 5mm |
| Type of Harmonics | Simple Harmonic Motion |
| Tentative “g” value | 0.1g-3g |
| Maximum Height of Models | 1500mm |
| Motor Rating | 10 HP, 3 Phase, 440 V Input |
| Control Panel Input Voltage | 4 Wire, 3 Phase, 440 V Input |

## 5.3 Model Description

### *5.3.1 Sand*

In all the tests, Guwahati Sand was used. The grading curve and geotechnical properties of the sand has been discussed in the chapter 2. The Fig 3.3 shows that the Guwahati sand falls within the zone of most liquefiable soils and therefore considered suitable for this study.

### *5.3.2 Container*

A transparent model container of size 550 x 500 x 500 mm with rigid boundary walls was fabricated using 12mm thick perspex sheets. The sheets were firmly glued with each other as well as encased in an aluminum frame consisting of aluminum angles. Fig. 5.5(a) and 5.4(b) shows the detailed schematic of the model and photographic view of the setup respectively. All the model tests were conducted in a 1-g environment (Iai 1989).

### *5.3.3 Back Saturation Arrangement*

A back saturation arrangement was provided at the base of the model to ensure complete saturation and internal homogeneity of the sand bed while keeping in mind the boundary drainage conditions while testing. The arrangement consisted of 6 water inlets at the bottom of the aluminum frame on the two opposite sides which were connected to a manifold through flexible pipes (shown in fig. 5.5(b)). A total 18 rubber supports were glued and fixed firmly at the base of the container. A perforated Perspex sheet was placed over the rubber supports which was sealed and secured from all four edges to restrict the movement of water through the sidewalls. Finally, a geotextile sheet was placed over the perforated sheet to ensure steady and uniform saturation.

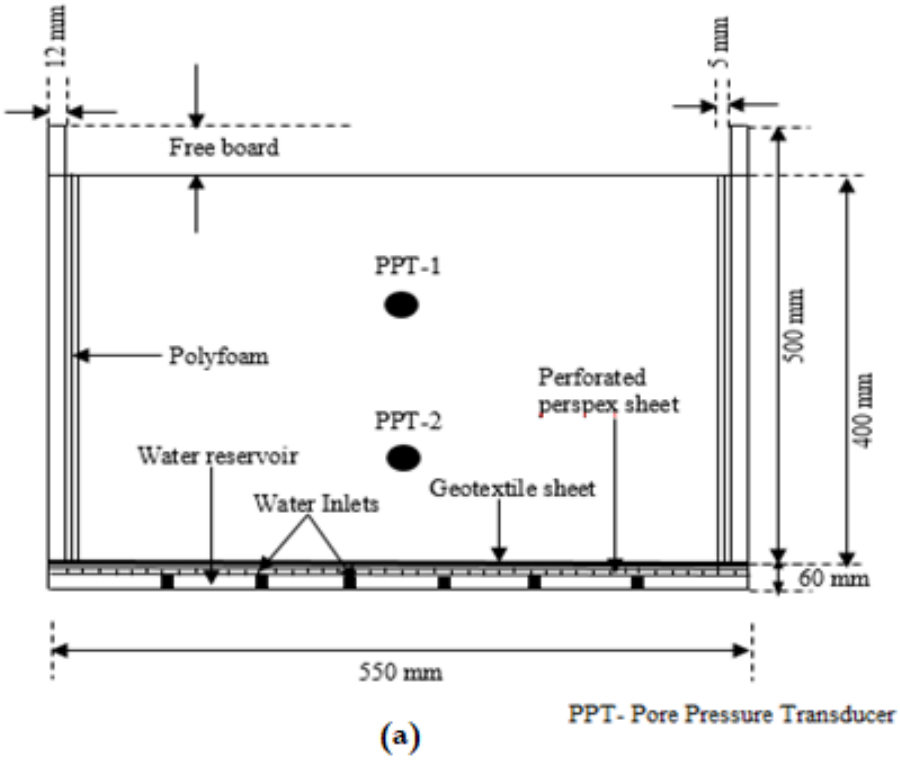


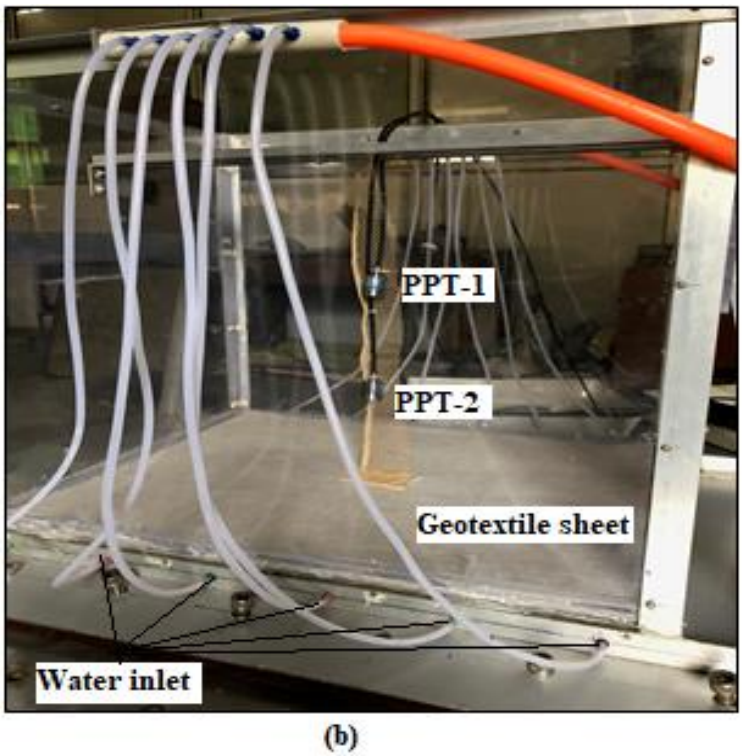


**Fig. 5.5 (a) Schematic diagram of test setup for shake table test (b) Experimental set-up on shake table**

However, the process of saturation through water in hydrocarbon contaminated sand was a challenging task. The hydrophobic property of hydrocarbons slowed the rate of saturation process, which was hindered even more as the oil content increased. To facilitate the saturation process, a small amount of dispersant was mixed with the water used for back saturation. The dispersant mainly constituted 2-[2-(4-nonylphenoxy) ethoxy] ethanol which is a highly surface active compounds and are capable of adding towards the solubilization and dispersion of water in oil which makes the saturation process faster. The concentration of dispersant in water was 0.0005 ml/L which is too low to cause any significant change in the pore pressure readings.

*5.3.4 Pore Pressure Sensors*

Two embedded type pore pressure sensors/transducers (PPT) (make BPR-A-S, FSO-50kpa) from PANATACHASIA with a rated capacity of 50kPa were used in this study (Fig. 5.6). The pore water pressure is measured by a flexible silicon diaphragm present in front of the PPT. The diaphragm is protected from the surrounding soil by a ceramic filter at its front that allows only pore fluid to get through it. Presence of any entrapped air in the top portion of ceramic filter will give erroneous readings. Therefore, it is important to ensure the full saturation of the filters before their installation as suggested by Take and Bolton (2002). The PPT was placed in an air tight saturation chamber which was filled with deionised water and connected to a vacuum pump.The PPT reading was monitored continuosly till it becomes constant. It took 30-45 minutes for the PPT to get completely saturated. Further, the sensors were checked for their response to the applied pressure, sensitivity, and return to zero reading after the load is removed. For this, sensors were housed in a small fluid calibration chamber which was attached to a constant pressure system as depicted in Fig. 5.7. The water pressure

was applied to the transducer in increments of 5 kPa up to a maximum value of 45 kPa. The pressure in the chamber was released from this maximum value in steps of 5kPa till zero. Once the fluid pressure had stabilized, readings were collected, usually in 30 s. On each transducer, a total of 5 loading/unloading pressure cycles were performed. The calibration parameters so obtained are indicated in Fig. 5.8. The non-linearity of both the transducers was found well within the acceptable limits.

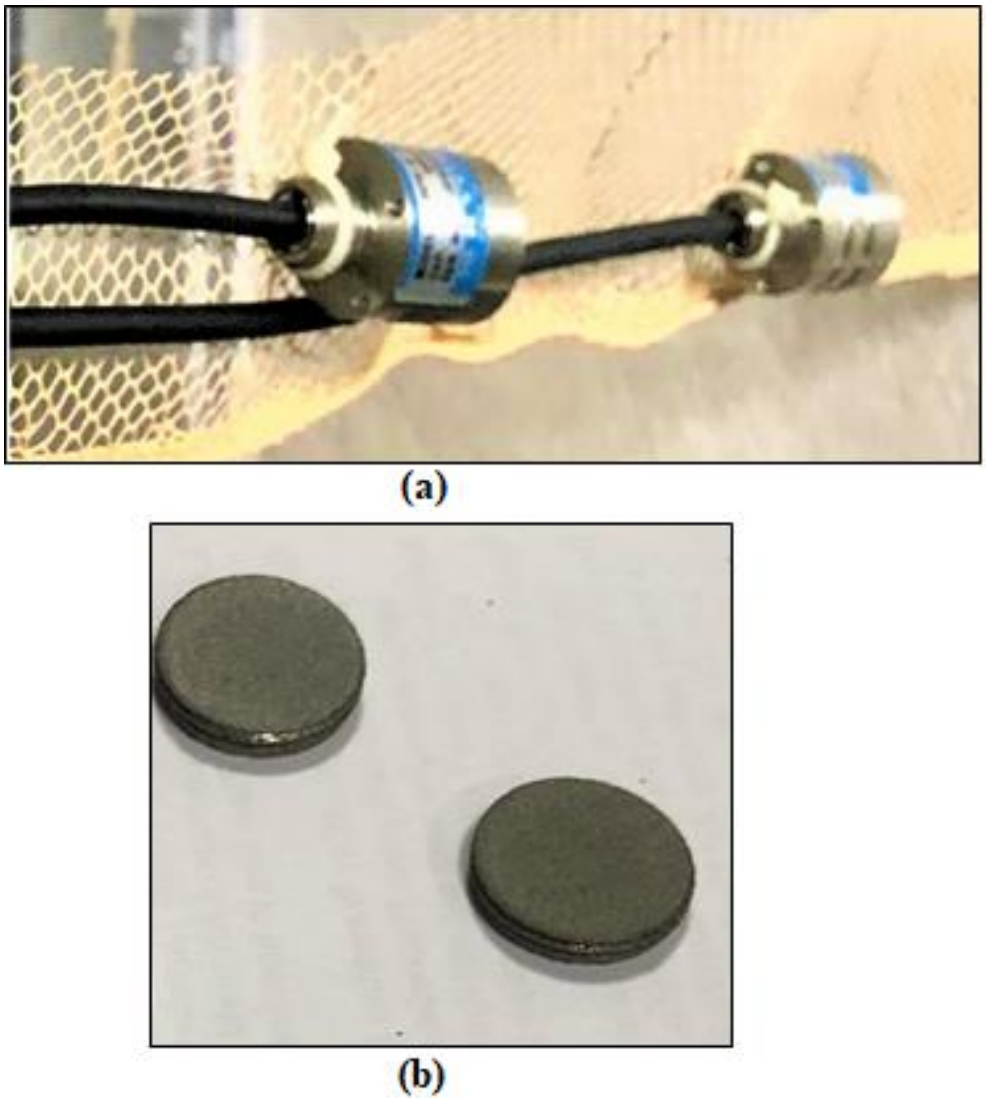


**Fig. 5.6 (a) Pore pressure transducers (b) Ceramic filters**

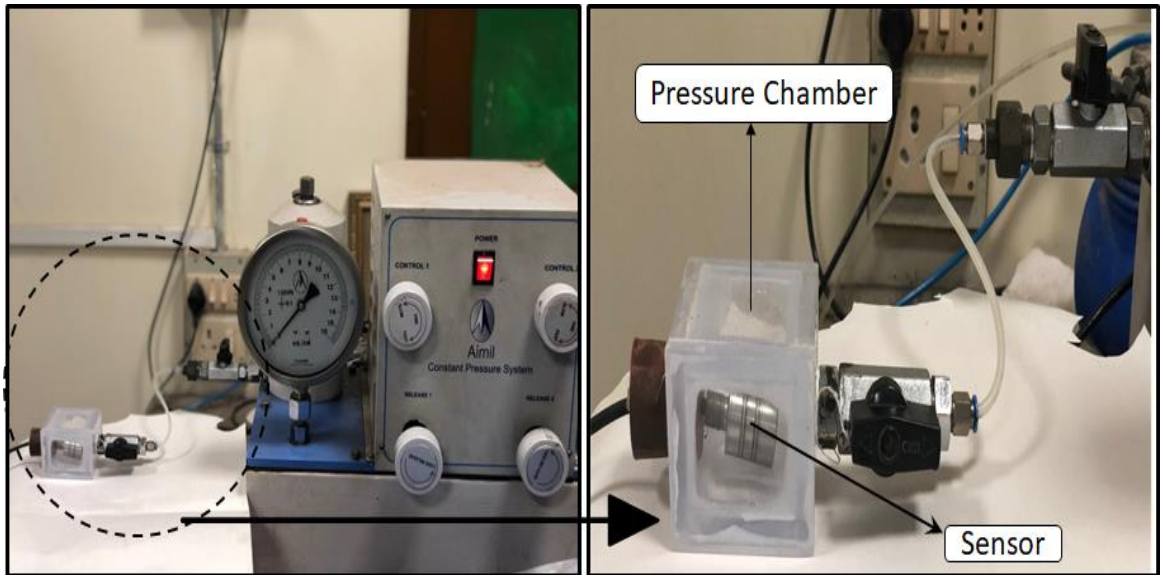


**Fig. 5.7 Pore Pressure transducer calibration chamber**

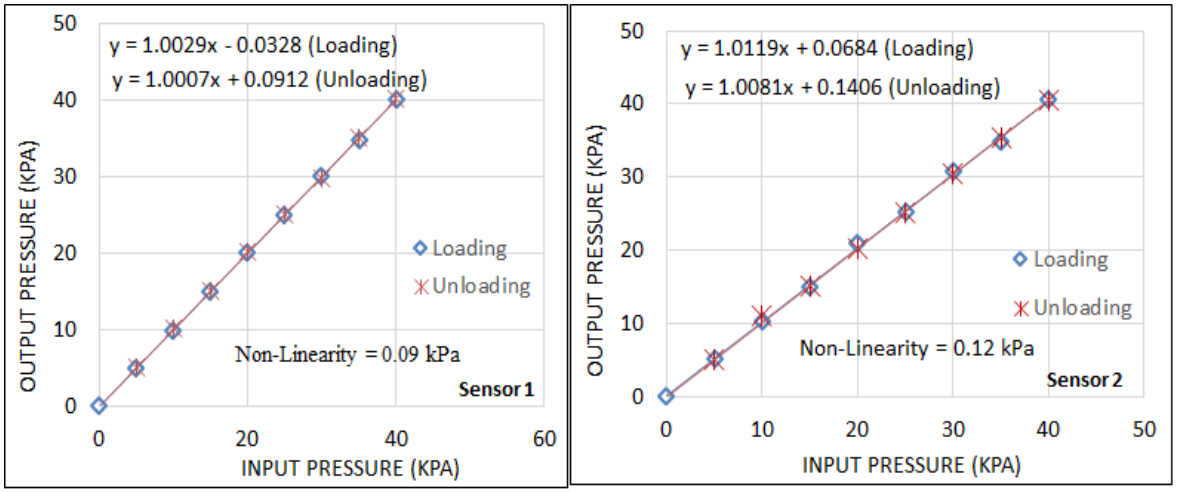


**Fig. 5.8 Calibration and performance check of pore pressure transducers**

*5.3.5 Accelerometer*

Two high sensitivity piezoelectric accelerometers from Brüel & Kjaer as shown in Fig. 5.9. were installed at container wall and Shake table (one each) to measure the acceleration in the direction of shaking. The sensitivity of the accelerometer was 100mV/g with a measuring range of ± 70g.

**Fig. 5.9 Accelerometers**

*5.3.6 Shake Table Performance*

In order to investigate the effect of mass of the model on the shaking system, a shake table test was conducted by loading the shake table with the empty model. Accelerometers were attached to the model wall and shake table (one each). The shake table was shaken with an external excitation of amplitude 5mm and frequency of 3.5 Hz. The result indicates that the acceleration recorded by both the accelerometers were nearly consistent (Fig. 5.10) and hence the effect of model inertia can be neglected.

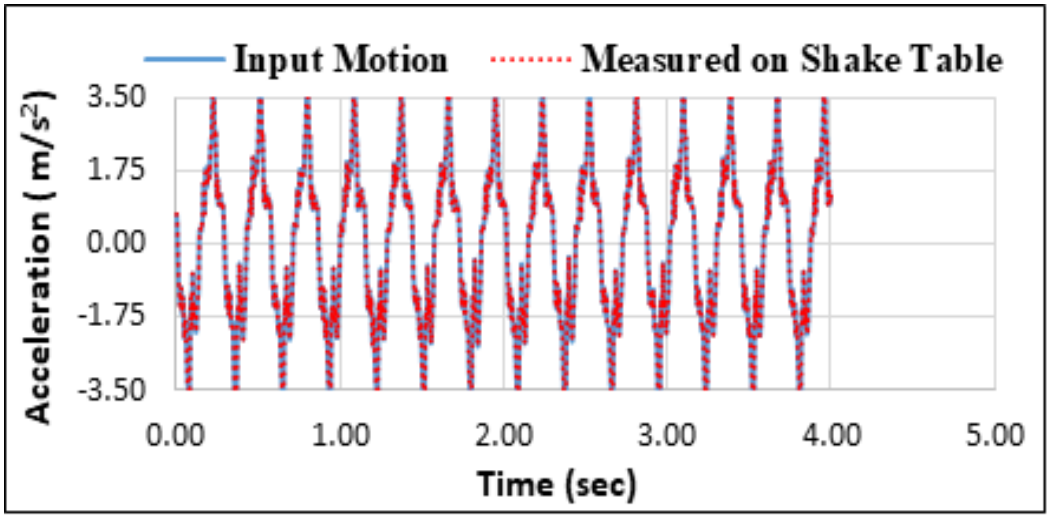


**Fig. 5.10 Base input acceleration and measured acceleration on shake table**

*5.3.7 Model Boundaries*

In the event of boundary processing, it is imperative to consider here that while replicating the laboratory scale dynamic soil performance studies, infinite boundary condition is one important requisite. Rigid boundary walls may not allow complete dissipation of energy associated with wave propagation and as a result, some of the waves may get reflected or scatter which may add inaccuracies in the anticipated response. Past experiments (Bhattacharya et al. 2011; Lombardi and Bhattacharya 2012), have shown that the presence of foam allows a certain amount of energy to be dissipated. Therefore, the sidewalls of the model were lined with a 5 mm thick foam.

## 5.4 Sample Preparation

Sample preparation is an important issue in any liquefaction analysis conducted using a shake table as any major non-uniformity in the density of the sand may impact the test results. Rainfall technique is generally preferred for cohesionless soils. Since, the present study deals with the sand containing hydrocarbon compounds, which induces a certain amount of apparent cohesion between the sand grains, moist-tamping method could have also been an option. Since, a loose sand bed with a target relative density of approximately 40% was required, moist tamping was not suitable. Therefore, separate density calibration curves were developed for different values of ω, shown in Fig. 5.12, and thereafter rainfall technique was adopted. To achieve this, an adjustable sieve arrangement was fabricated (shown in Fig. 5.11). A mould was placed below the sieve and sand was rained from different heights (increments of 10cm) by adjusting the height of the sieve. The density achieved corresponding to each height was noted and a curve was plotted between density and height of fall. It was observed that the density increases with increasing the height of fall. In some cases, it became constant after a certain height.

**Fig. 5.11 Adjustable sieve arrangement for rainfall technique**

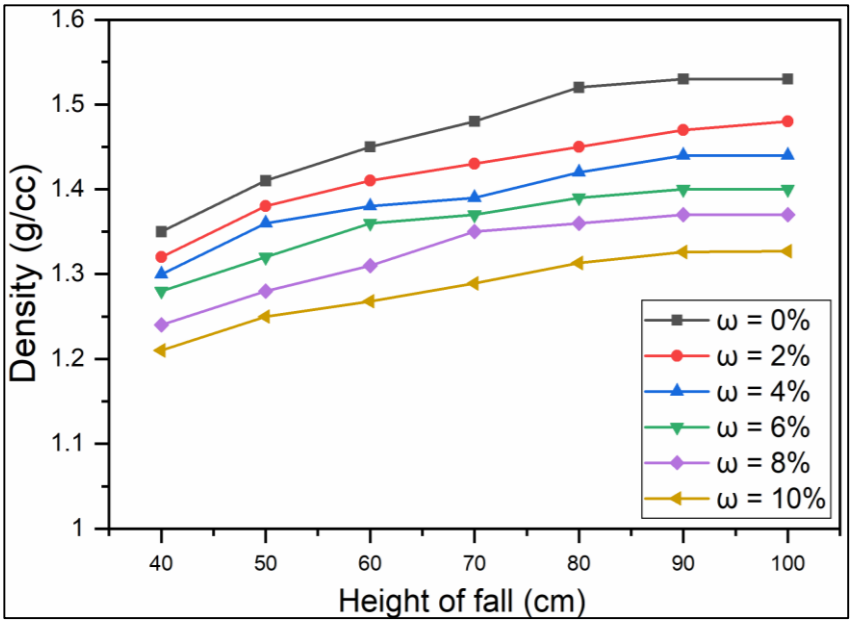


**Fig. 5.12 Density calibration curves for uncontaminated and contaminated sand**

Before raining the sand into the testing tank, the pore pressure transducers were installed at the center of the tank for minimal boundary effect at a depth of 15cm and 30cm. Prior to installation in the testing tank, the pore pressure sensors were tied on a supporting net to allow minimal disturbance in their position while shaking. The sand was poured through the sieve into the tank. The deposition intensity and the drop height were strictly controlled to achieve a uniform sand profile with an average relative density of 40%. A 400 mm high sand bed was prepared which was then subjected to back saturation with the help of 12 water inlets provided at the bottom of the model tank. The saturation stage lasted for 15-20 hrs and full saturation state was marked by appearance of a thin water film over the sand bed. Sand contaminated with higher percentages of crude oil took a longer time to saturate due to the hydrophobic nature of oil. The amount of water introduced into the sand was strictly monitored to ensure full saturation stage. All the liquefaction tests are conducted with water table maintained at the top surface of the sand bed.

### 5.5 Signal Conditioning and Data Acquisition System

Two separate Data Acquisition systems were used for data logging through the pore pressure transducers and accelerometer. A 3-channel Krypton Data Acquisition system (shown in Fig 5.13) supported with an interface software DEWESOFT was used for data logging from pore pressure transducers. The sampling rate was maintained at 500 Hz. A typical logging interface has been depicted in Fig. 5.14. In order to eliminate the noise, Butterworth low pass filter of sixth order was applied on the raw recorded data as shown in Fig. 5.15. The excess pore pressure data obtained after application of filter is shown in Fig. 5.16.


**Fig. 5.13 Krypton-3-STG Data acquisition system**

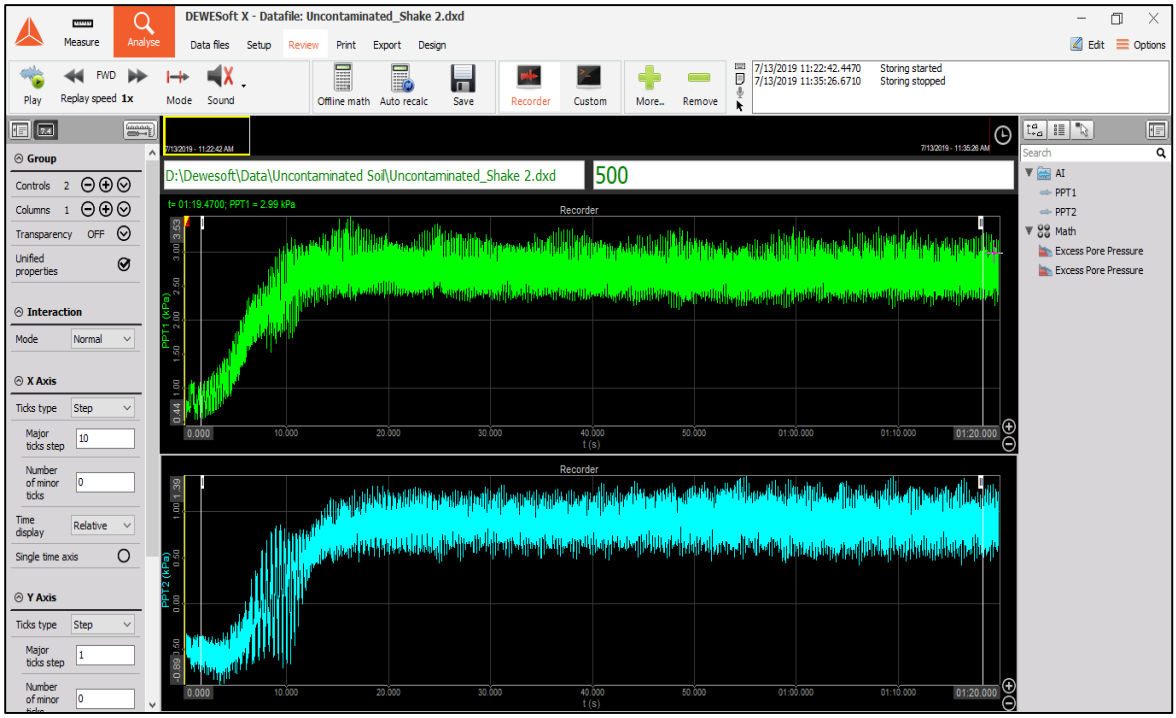


**Fig. 5.14 Typical DEWESOFT interface showing excess pore pressure data without filter**

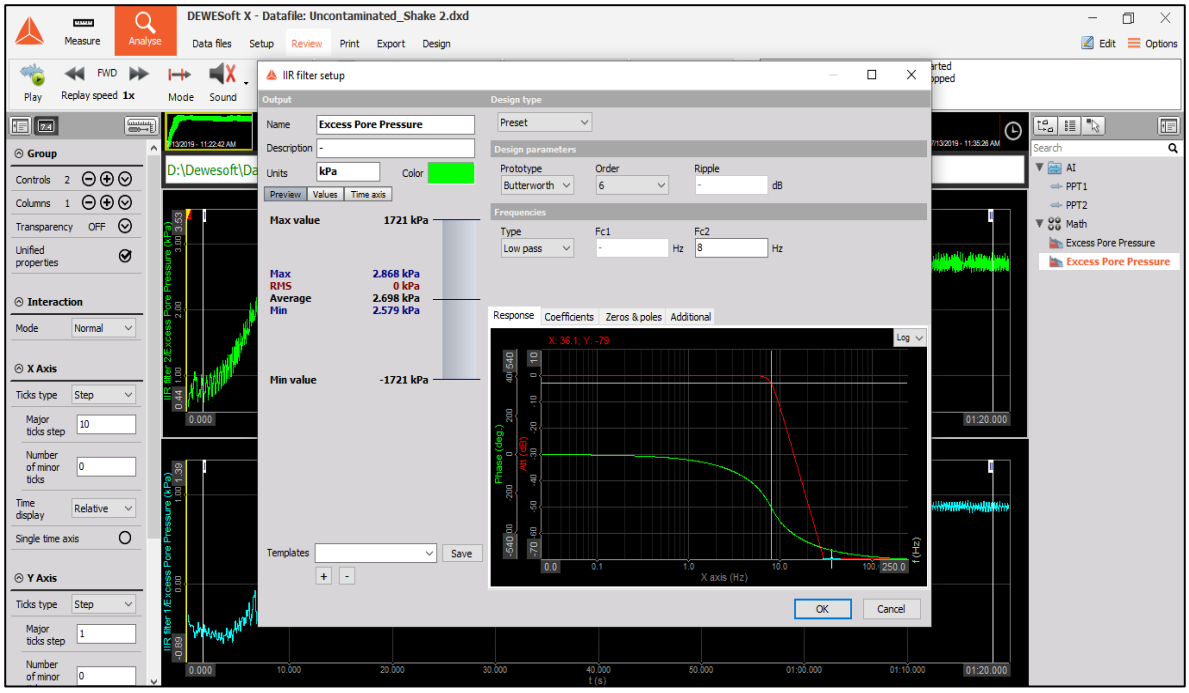


**Fig. 5.15 Filter application after data logging in DEWESOFT**

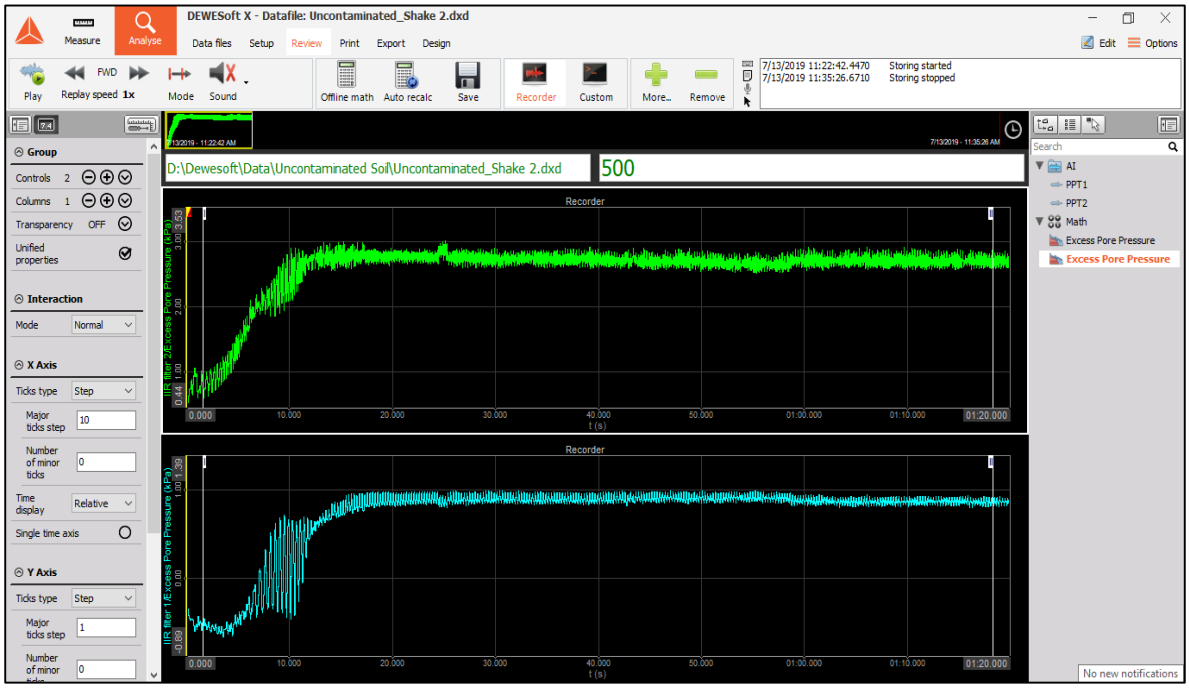


**Fig. 5.16 Excess pore pressure data after filter application**

Further, for accelerometers, a 6-channel Brüel & Kjaer Data Acquisition System with Labview software interface was used for data logging.

## 5.6 Test Results

### *5.6.1 Influence of Hydrocarbon on Pore Pressure Response of Guwahati Sand*

The presence of hydrocarbon compounds in the soil matrix has a significant effect on the development of cyclic pore pressure by altering the physio-chemical properties of sand as well as pore fluid. Oil contamination also transforms the soil-water characteristic curve (SWCC) by changing the matric suction values. However, this particular aspect has not been considered here, as all the tests in this study has been considered to be conducted at fully saturated state at which the matric suction is negligible.

To study the effect of the presence of hydrocarbon compounds on the liquefaction potential of Guwahati sand, shake table tests were conducted with varying percentages of crude oil, ω, (0%, 2%, 4%, 6%, 8% and 10%) subjected to a base shaking of 0.35g. The pore pressure-time histories recorded at two different depths i.e., d= 30cm and d=15 cm within the sand bed for three consecutive shakings have been presented in Fig. 5.17 and Fig. 5.18, respectively. From Fig. 5.17, it can be seen that the magnitude of excess pore pressure, Δu was reduced moderately with the initial increase in ω up to 6%. This reduction in Δu was more significant at lower oil contents. During first shaking event, the value of maximum excess pore pressure, $\Delta u_{max}$, at d = 30cm was reduced by 24.36%, 18% and 8.2% when ω was varied from 0% to 2%, 2% to 4% and 4% to 6% respectively. Beyond ω = 6%, a sharp increase was experienced in the value of $\Delta u_{max}$. For ω = 10%, the value of $\Delta u_{max}$ surpassed the value observed for clean sand. A substantial increase of 63% observed in value of $\Delta u_{max}$ when ω was increased from 6% to 10% indicates a drastic increase in liquefaction potential. However, this trend can be more accurately understood in terms of normalized excess pore

pressure values as the presence of crude oil also impacts the effective overburden stresses which will be different for each case.

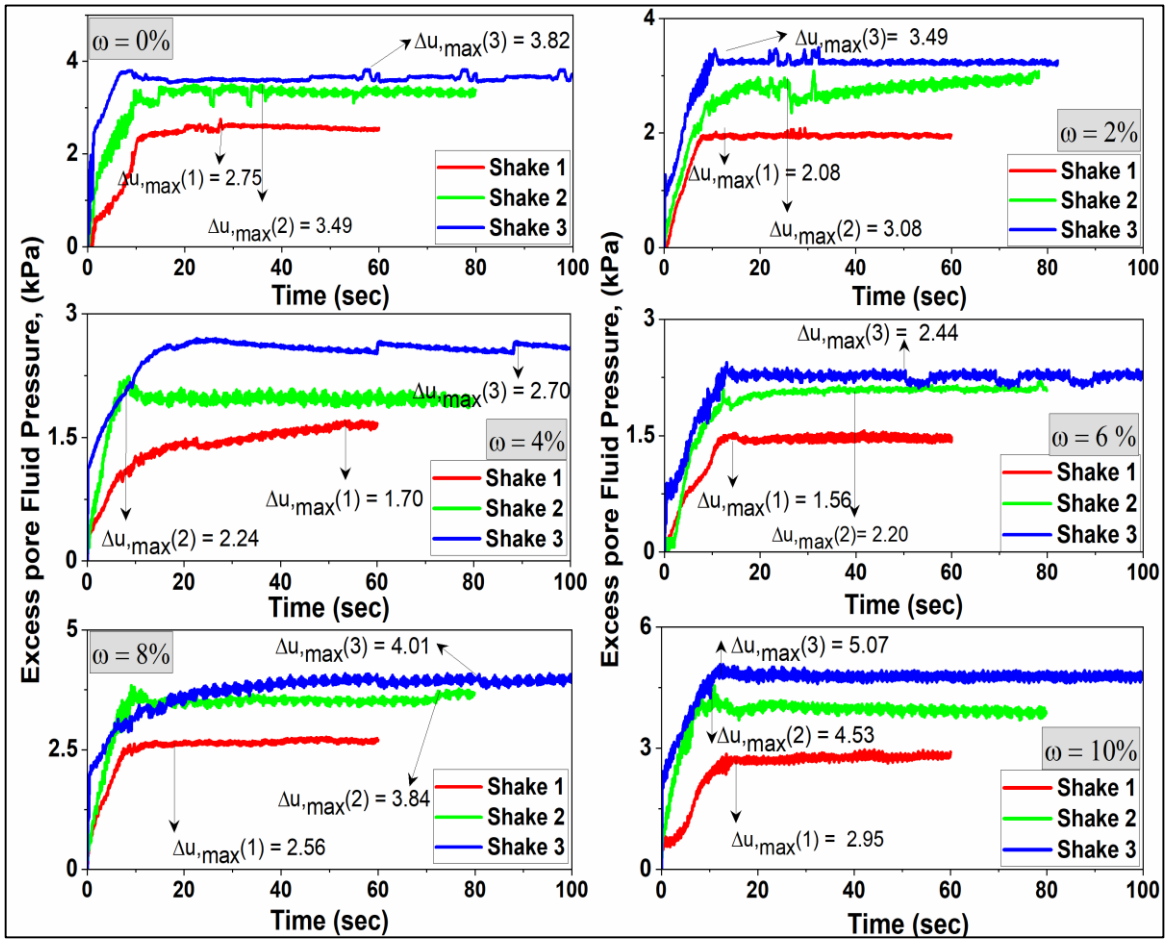


**Fig. 5.17 Excess pore pressure-time histories at varying oil dosages for three shaking events at d=30 cm**

In view of the effect of shaking history on liquefaction potential, it is also worth noticing that the history of shakings tends to reduce the susceptibility of sand bed towards liquefaction due to the densification effect. The value of $\Delta u_{max}$ was increased for each subsequent shaking irrespective of the value of ω. For crude oil-contaminated sand beds, the increase in the value of $\Delta u_{max}$ from shake 1 to shake 3 lied in the range of 56-70%. On the other hand, this increase was only 38% for uncontaminated sands. This observation can be explained through the lubricating effect of crude oil due to which higher degree of

densification and thus higher levels of pore pressure was achieved. No such effect was possible in uncontaminated sands. However, there was a remarkable gain in the liquefaction resistance with each subsequent shaking indicated by the values of the pore pressure ratio. This was again due to the greater values overburden stresses generated in the densified sand. Moreover, being lighter than water, shaking causes the displacement of oil in the soil pores by water resulting into the diminished effect of oil contamination on sand behavior during further shaking events. Similar implications can be drawn from the pore pressure-time histories recorded at d = 15cm, shown in Fig. 5.18. The magnitude of $\Delta u_{max}$ at 15 cm depth was lower than those observed at 30 cm depth.

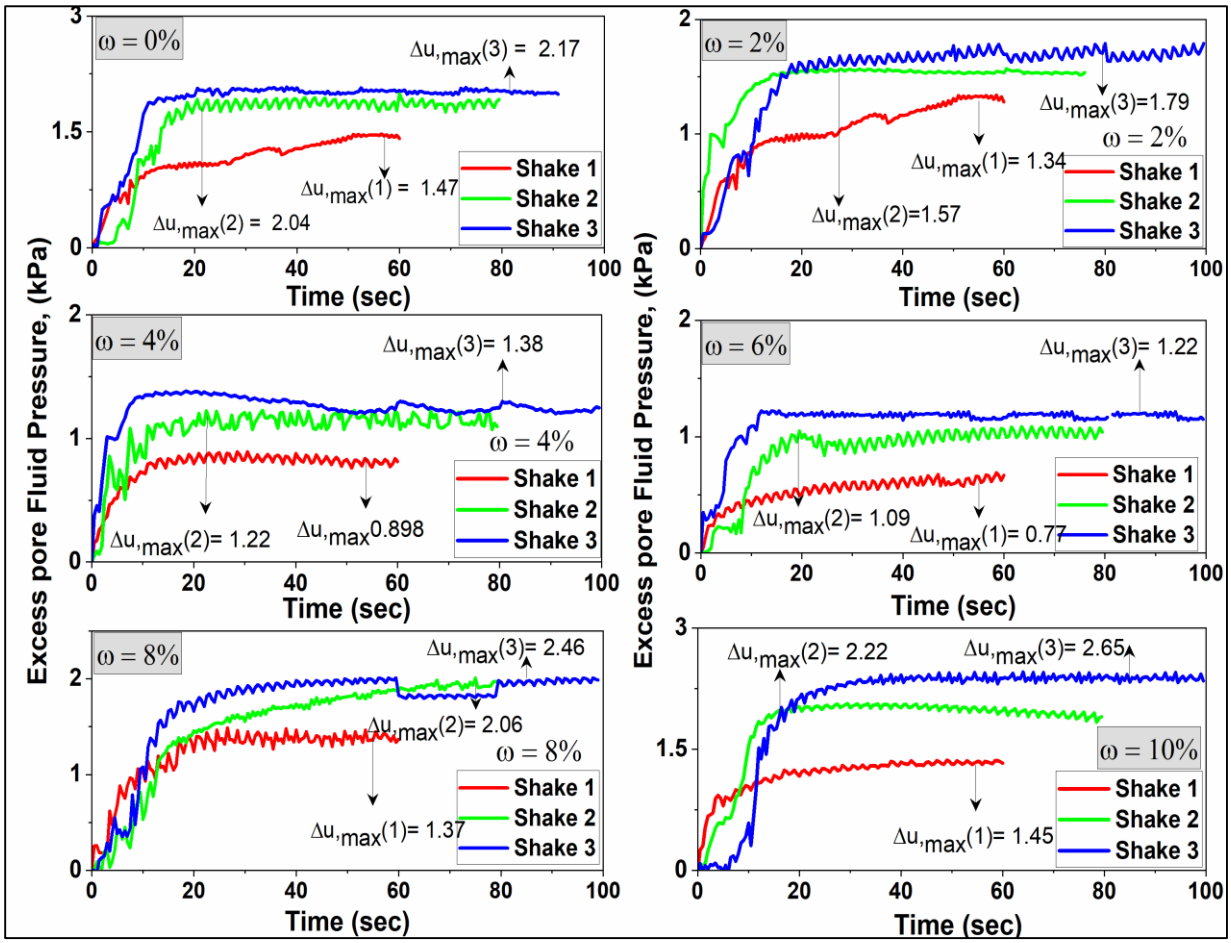


**Fig. 5.18 Excess pore pressure-time histories at varying oil dosages for three shaking events at d=15 cm**

The decline in the values of $\Delta u_{max}$ with initial increase in ω are comparable with the values observed at d = 30cm. Shaking events had a more pronounced effect on $\Delta u_{max}$ at d = 15cm. The percentage increase in $\Delta u_{max}$ from shake 1 to shake 3 attained a value as high as 79% and 82% for ω = 8% and 10% respectively which are significantly higher than 56% and 70% observed at d = 30cm for respective ω values. This can be attributed to the fact that sand bed at shallower depths being comparatively loose due to absence of overburden effect have a higher scope to densify which is also accompanied with the lubricating effect of crude oil.

The effect of crude oil contamination on the liquefaction potential of Guwahati sand can be more appropriately understood in terms of normalized excess pore pressure also known as pore pressure ratio, $r_u$. Pore pressure ratio can be defined as the ratio of excess pore pressure to the effective overburden stress. The soil will be said to be in liquefied stage when $r_u$ equals to unity. However, in the present study, the point at which the $r_u \approx 0.88$ (Ishihara, 1993) has been considered as the point of initiation of liquefaction. Fig. 5.19 shows the comparative schematic of the various states of liquefaction achieved in terms of normalized pore pressure for varying oil dosages at both d = 30cm and d = 15cm. The figure also gives a comparison of time elapsed before the onset of liquefaction. The trend of $r_u$ during shake 1 was similar to that of excess pore pressure. At d = 30cm, the maximum value of $r_u$ dropped from 0.98 to 0.91 when ω increased from 0% to 2%. Furthermore, the time required for initiation of liquefaction, $T_{L,}$ was increased from 27.4 sec for ω = 0% to 29.8 sec for ω = 2%. While no liquefaction was observed for ω= 4% and 6% during shake 1, complete liquefaction ($r_u$ = 1) was evitable for 8% and 10% contaminated sand within 19 seconds and 13.5 seconds respectively. The variation of liquefaction susceptibility with crude oil content at 15cm depth was analogous to the one observed at 30cm depth during shake 1. Although the magnitude

of the pore pressure ratio observed at 15 cm was higher than at 30 cm owing to lesser effective overburden stress, the time required for the onset of liquefaction was more at 15cm depth. This implies the movement of pore fluid pressure from bottom to top. Hence from the above discussion, it can be inferred that the presence of crude oil moderately increased the liquefaction resistance till $\omega \leq 6$ %. The instant $\omega$ becomes greater than 6 %, the liquefaction resistance begins to falloff remarkably, and for $\omega = 10\%$, it experiences a value lower than that of virgin sand. Hence the variation of liquefaction resistance with crude oil content results into a single-peaked profile with maximum value observed at $\omega = 6\%$. Likewise, on the basis of maximum pore pressure values observed during the second and third shaking event, it was seen that the maximum resistance was observed at $\omega = 6\%$ only. Although, in any case, no liquefaction was observed during shake 3 due to sufficient densification of the sand bed. Hence from above observation, $\omega = 6\%$ can be regarded as the threshold point from where the liquefaction behavior of oil-contaminated sand was reversed.

There can be two underlying mechanisms that might be supposed to independently govern the pore pressure behavior of oil-contaminated Guwahati sand above and below the threshold point respectively. The first mechanism owes to the difference in the bulk modulus of the pore fluids which is dominant at lower oil contents. At lower degrees of contamination, the amount of crude oil is insufficient to completely coat the sand grains and it occupies the inter-granular voids in the form of oil droplets as can be seen from the SEM images in Fig.3.10. Consequently, the grain to grain contact still exists and there appears to be a negligible loss of effective stress. Moreover, it is also evident from the previous studies (Khamehchiyan et al. 2007) that oil contamination induces an apparent cohesion due to pore-fluid viscosity which will again be helpful in holding the soil matrix intact. The pore fluid

pressure generation in such a case would be from the combined effect of oil and water. Since the bulk modulus of oil is lower than that of water, the pressure generated by oil would be lesser than water. This explains the reduction in the pore pressure and hence increase in liquefaction resistance with initial contamination of $\omega \leq 6\%$.

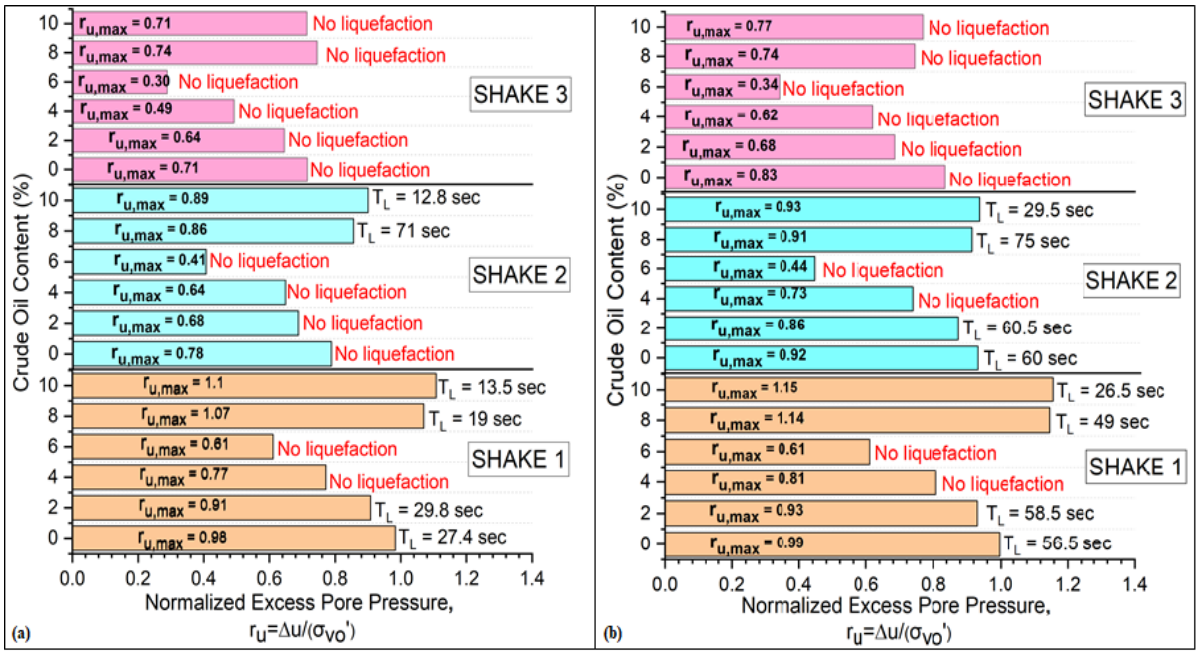


**Fig. 5.19 Comparison of maximum excess pore pressure ratio, $r_{u,max}$ and time to liquefaction, $T_L$ for homogenous sand bed at (a) d = 30cm and (b) d = 15cm**

The second mechanism explains the behavior observed beyond $\omega = 6\%$. At higher degrees of contamination, the sand grains get completely smeared with a hydrocarbon layer and fill the micro and macro pores of the soil as well. Consequently, it can effectively decompose the inter-particle contact friction and the majority of soil grains would lose their contacts with neighboring grains. Moreover, the effective stress resulting from the grain-to-grain contact surface also gets lost which in turn reduces the liquefaction resistance. Hence it can be inferred that at lower oil content, compressibility characteristics of pore fluid dominates while at higher oil content frictional characteristics of sand grains dominate.

*5.6.2 Cone Penetration Index and DPI Recovery*

As per the schedule of the multiple shaking events, a series of CPT tests were conducted on the sand specimen across different shaking events to obtain the relative compactness along the sand bed with different shaking events. The relative compactness indicated by the DPI values were plotted along the depth for the three shaking events and different oil contents which has been shown in Fig 5.20. It was observed that for ω = 0%, CPT1 have almost similar DPI along the depth (slightly decreased at the bottom due to overburden effect), indicating homogeneous sample preparation. CPT 2 and CPT 3 showed an obvious decrease in DPI and hence an improved strength as compared to the initial condition for all values of ω. Liquefaction disturbed the existing soil structure significantly and thus reduced the cone resistance immediately after the shaking. Hence, both shaking disturbance and sand densification affected the cone resistance variation before and after shaking Further, it can be observed that the DPI profile corresponding to shake 2 lies closer to DPI profile of shake 3 as compared to the shake 1 indicating that the major portion of the settlement was achieved after the first shaking itself. Furthermore, it was also evident that the oil contaminated sand bed showed a higher DPI than the uncontaminated bed. The increase in the value of DPI was directly proportional to the value of ω i.e, higher the value of ω, higher was the DPI value. The behavior was valid for all three CPTs.

This observation can be explained by the lubricating effect of oil which causes more penetration with each blow. The densification of sand bed indicated by the reduced DPI explains the reduction in liquefaction potential with each shaking event. However, it is important to mention here that there these DPI values does not directly estimate the liquefaction potential but they provide an indicative assessment for the same.

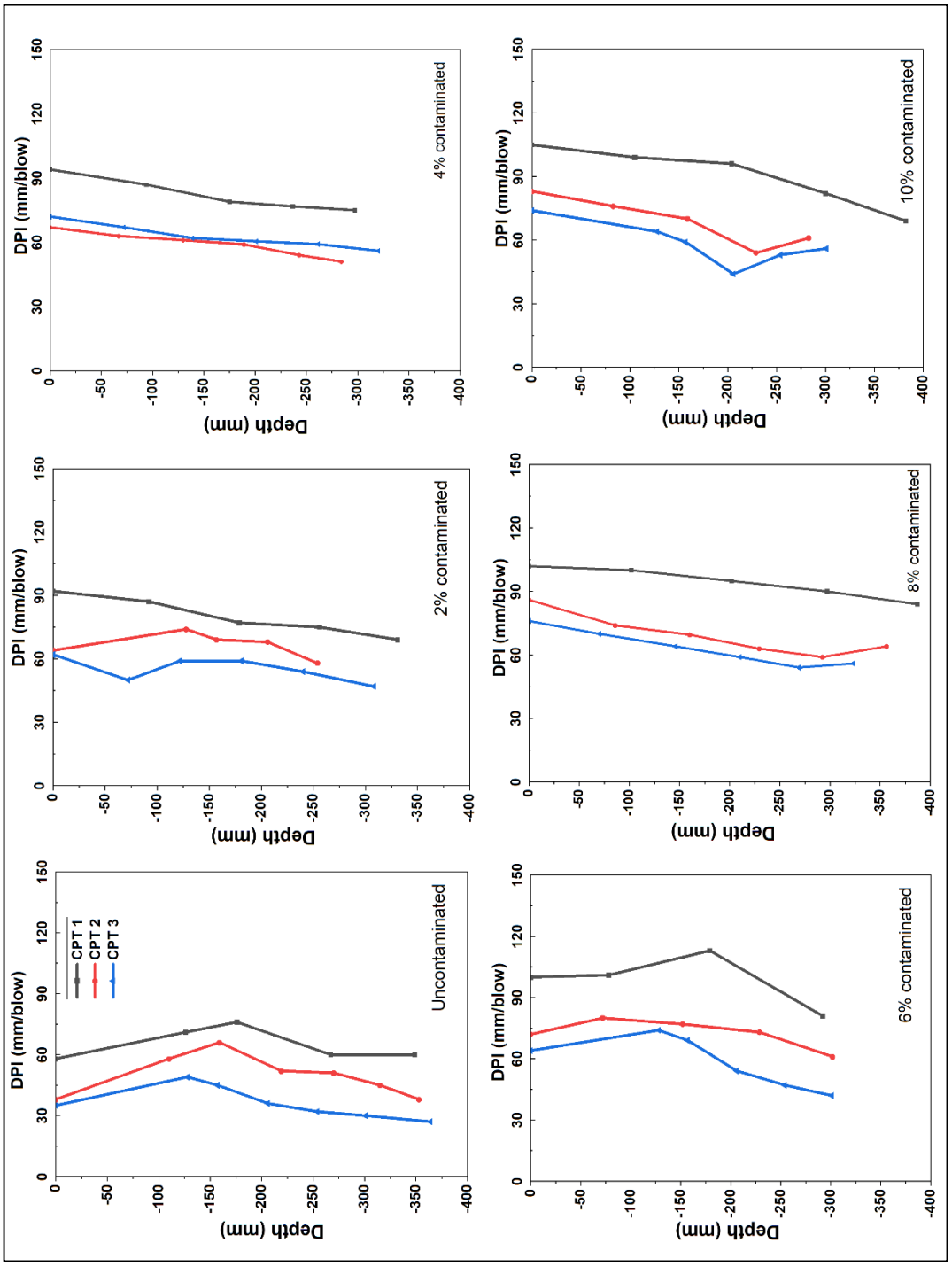


**Fig. 5.20 Cone Penetration Test results before and after shaking events**

Although liquefaction reduces the cone resistance initially, but with time as pore pressure dissipates, soil regain its strength. This section investigates the extent upto which the sand could recover its strength post liquefaction. This recovery can be expressed as eq. (5.1)

$$DPI_{recovery} = \frac{DPI_{CPT1} - DPI_{CPTi(i=2-3)}}{DPI_{CPT1}} \text{ x } 100\% \quad (5.1)$$

The DPI values have been averaged over the entire depth and average value of CPT 1 prior to liquefaction is considered as a base value. The calculated percentages of $DPI_{recovery}$ have been illustrated in Fig. 5.21. The horizontal zero line represents the pre-liquefaction DPI.

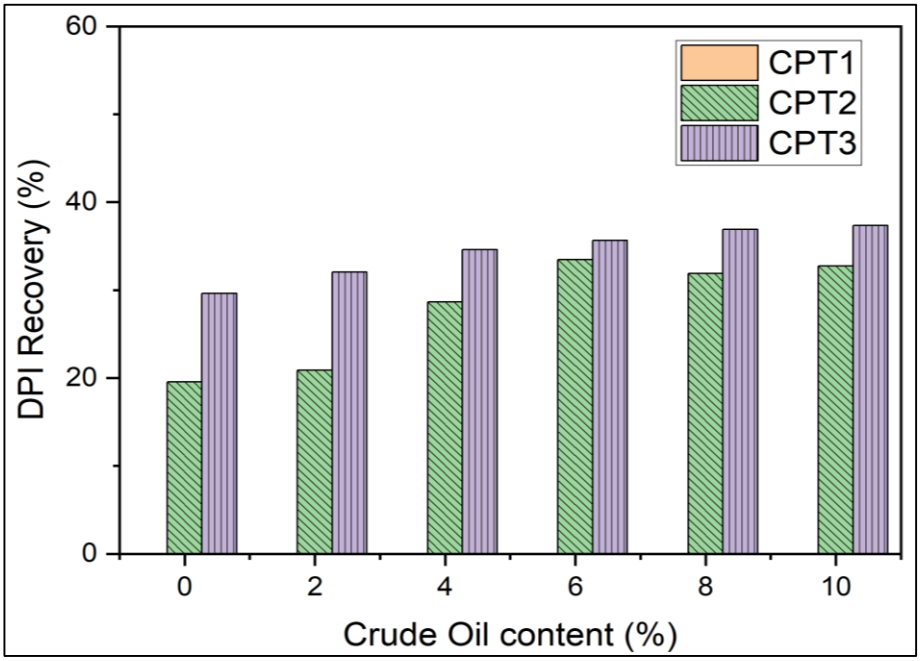


**Fig. 5.21 Variation of DPI Recovery with oil content**

For ω = 0%, CPT-2 showed 19.55% increase while CPT-3 showed 29.62% increase compare to CPT-1. Similarly, for ω = 2% CPT-2 showed 20.87% increase while CPT-3 showed 32.04% increase. The difference in the DPI recovery during CPT-2 and CPT-3 tends to reduce with increasing ω. However, the percentage value of DPI recovery was constantly increasing with increasing oil content. These observations can be attributed to the lubricating effect of oil which causes densification to a greater extent when ω is high. The DPI recovery reached the value as high as 32.7% and 37.32% for CPT-2 and CPT-3 respectively when ω = 10%.

*5.6.3 Effect of Depth of Contamination on Pore Pressure Response*

The effect of depth of contamination was studied in terms of contamination depth ratio (β), which has been defined as the ratio of contamination depth to the total considered depth which is 40cm in the present study. The study accounts for β = 0, 0.356, 0.55, 0.75 and 1 where β = 0 refers to uncontaminated homogeneous sand bed while β = 1 refers to contaminated homogeneous sand bed at varying oil contents. Further experiments were conducted for β = 0.356, 0.55 and 0.75 to take into account the influence of contamination depth on liquefaction potential of the sand bed. Fig. 5.22 shows a schematic representation of the layered sand in the model tank. The positions of both the pore pressure transducers remain unchanged i.e., 15cm and 30 cm.

Fig. 5.23 and Fig. 5.24 shows the excess pore pressure data for β = 0.356 at 30 cm and 15cm depth respectively for varying oil dosages and shaking events. The behavior during the second shaking event lies in between the first and third shaking events as observed in the case of homogeneous sand beds. Excess pore pressure trend with increasing oil dosages was diametrically affected by the behavior of homogeneously contaminated sand bed. The value of excess pore fluid pressure showed a decreasing trend with increasing ω for ω ≤ 6% while a reversed trend was observed for ω > 6%. For β = 0.356, the value of $\Delta u_{max}$ at d = 30cm dropped from 2.57 kPa to 2.09 kPa for shake 1, 3.23 kPa to 2.70 kPa for shake 2 and 3.72kPa to 3.05 kPa shake 3 when the value of ω increased from 2% to 6%. Thereafter, $\Delta u_{max}$ increased correspondingly from 2.09 kPa to 2.65 kPa, 2.70 kPa to 3.60 kPa and 3.05 kPa to 4.20 kPa when ω increased from 6% to 10%. Likewise, the value of $\Delta u_{max}$ at d = 15cm dropped from 1.42 kPa to 1.15 kPa for shake 1, 1.74 kPa to 1.39 kPa for shake 2 and 1.74 kPa to 1.39 kPa for shake 3 when the value of ω increased from 2% to 6% and thereafter

rose to 1.48 kPa, 1.74 kPa and 1.98 kPa for shake 1, shake 2 and shake 3 respectively when ω was increased to 10%.

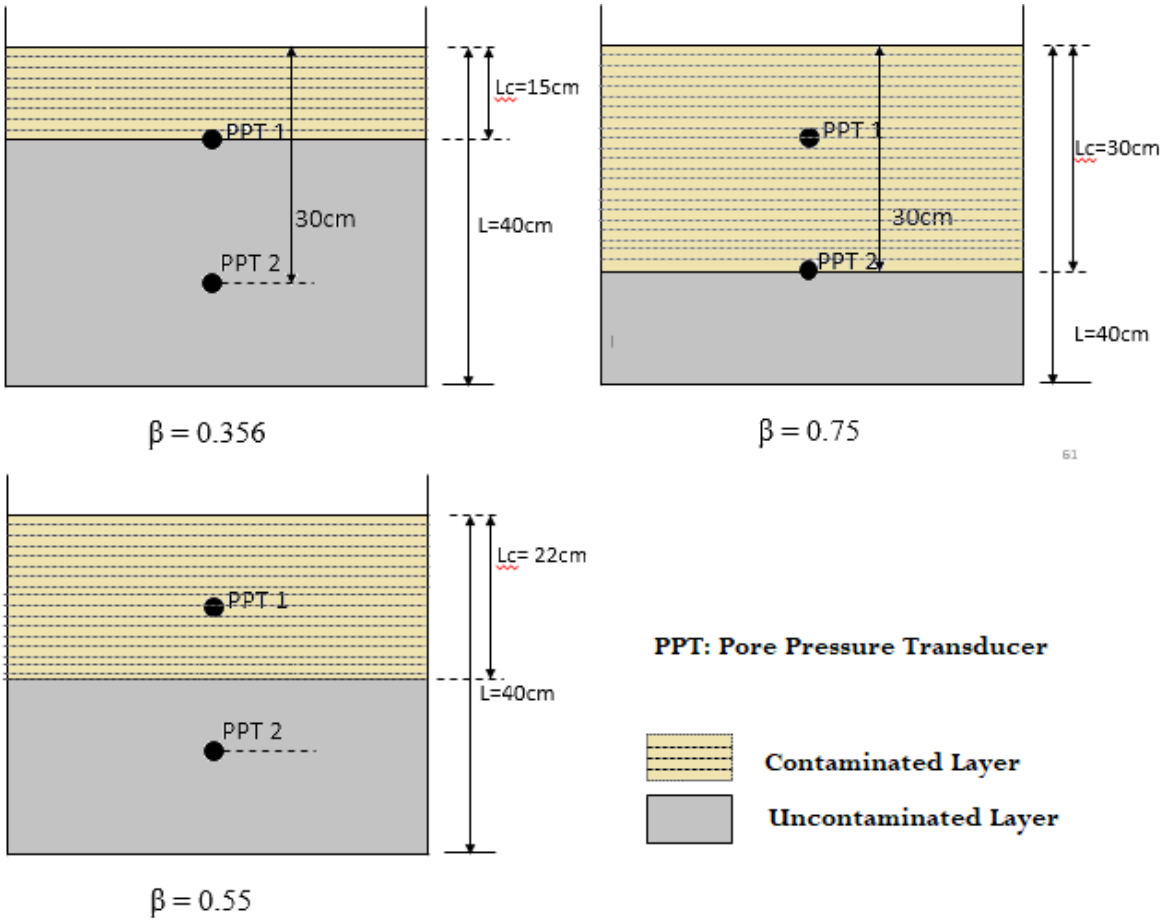


**Fig. 5.22 Schematic view of preparation of layered sand bed**

Similarly, Figs.5.25 and Fig. 5.26 shows the pore pressure-time history data recorded for β = 0.55 for d = 30 cm and d = 15 cm respectively. For β = 0.55, the value of $\Delta u_{max}$ at d = 30cm was dropped from 2.39 kPa to 1.80 kPa for shake 1, 3.21 kPa to 2.59 kPa for shake 2 and 3.62 kPa to 2.64 kPa for shake 3 when ω increased from 2% to 6%. With further increase in ω from 6% to 10%, $\Delta u_{max}$ increased from 1.8 kPa to 2.69 kPa, 2.5 kPa to 3.69 kPa and 2.64 kPa to 4.46 kPa for shake 1, shake 2 and shake 3 respectively. Likewise, from Fig 5. 27 and Fig. 5.28, it was observed that for β = 0.75, the value of $\Delta u_{max}$ at d = 30cm declined

from 2.39 kPa to 1.80 kPa for shake 1, 3.22 kPa to 2.48 kPa for shake 2 and 3.64 kPa to 2.64 kPa for shake 3 when ω increased from 2% to 6%. Yet again, with further addition of oil from 6% to 10%, $\Delta u_{max}$ increased from 1.8 kPa to 2.64 kPa, 2.48 kPa to 3.80 kPa and 2.64 kPa to 4.46 kPa for shake 1, shake 2 and shake 3 respectively. Consistent findings have also been recorded at d = 15 cm for both β = 0.55 and 0.75, as per the observed patterns discussed above at d = 30cm. For β = 0.55, the value of $\Delta u_{max}$ at d = 15cm dropped from 1.38 kPa to 1.09 kPa for shake 1, 1.70 kPa to 1.34 kPa for shake 2 and 1.89 kPa to 1.58 kPa for shake 3 when the value of ω increased from 2% to 6% and thereafter rose to 1.91 kPa, 1.96 kPa and 2.85 kPa for shake 1, shake 2 and shake 3 respectively when ω was increased to 10%. Similarly, for β = 0.75 and d = 15 cm, the value of $\Delta u_{max}$ declined from 1.51 kPa to 1.06 kPa for shake 1, 1.69 kPa to 1.31 kPa for shake 2 and 1.98 kPa to 1.45 kPa for shake 3 when ω increased from 2% to 6%. With further addition of oil from 6% to 10%, $\Delta u_{max}$ increased from 1.06 kPa to 1.48 kPa, 1.31 kPa to 2.13 kPa and 1.45 kPa to 2.33 kPa for shake 1, shake 2 and shake 3 respectively.

Apart from the magnitude of excess pore fluid pressure, it can also be pointed out that the presence of crude oil does not significantly affect the rate of development of pore pressure initially. However, shaking history does affect the rate of building up of pore pressure. It is also evident from the figures that the rate of growth of pore pressure at shallow depth was slower relative to the one found at deeper depths, regardless of the values of ω and β.

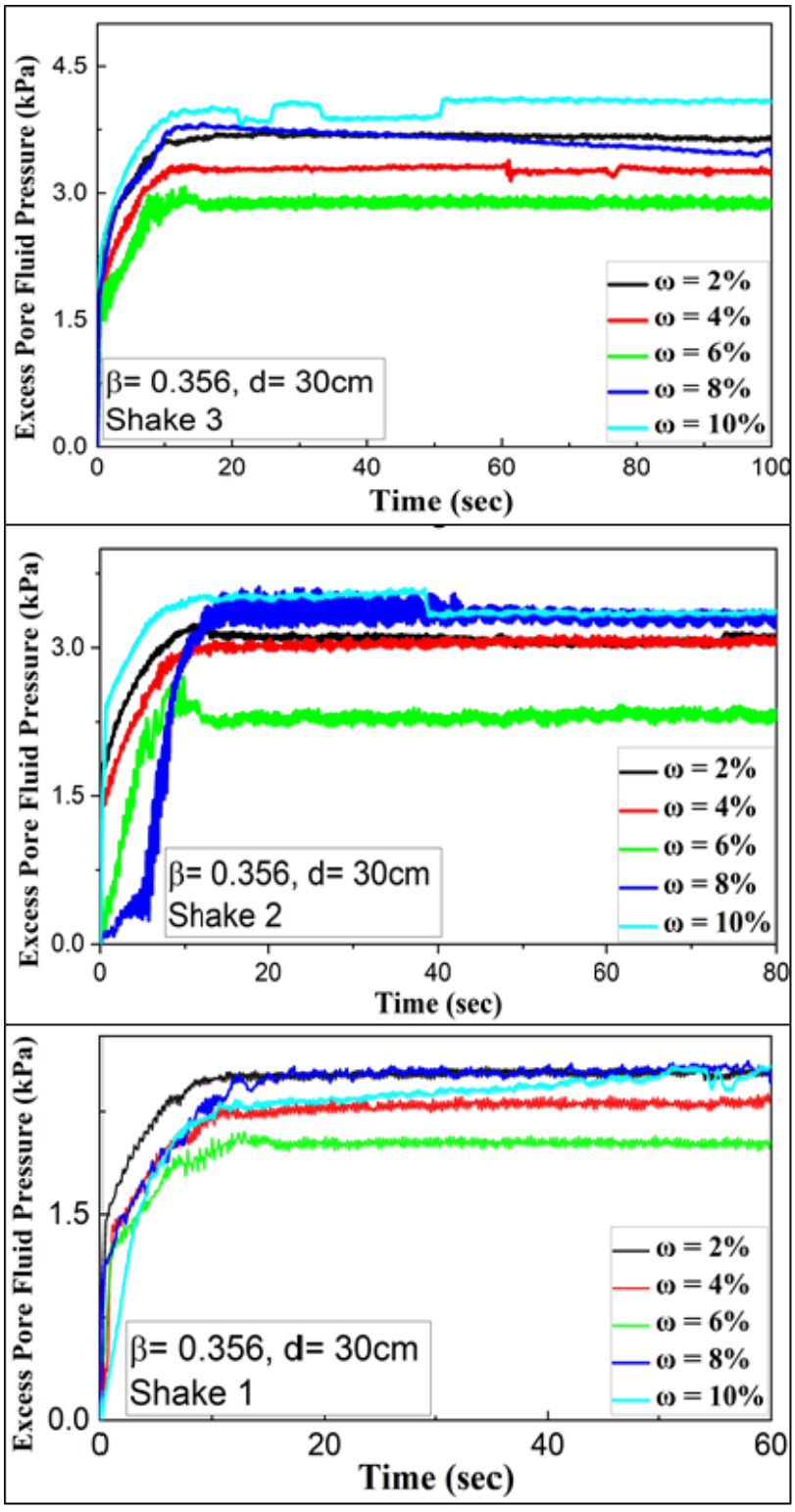


**Fig. 5.23 Excess pore pressure-time histories for different shaking events at varying oil content, ω, for β = 0.356 and d= 30cm**

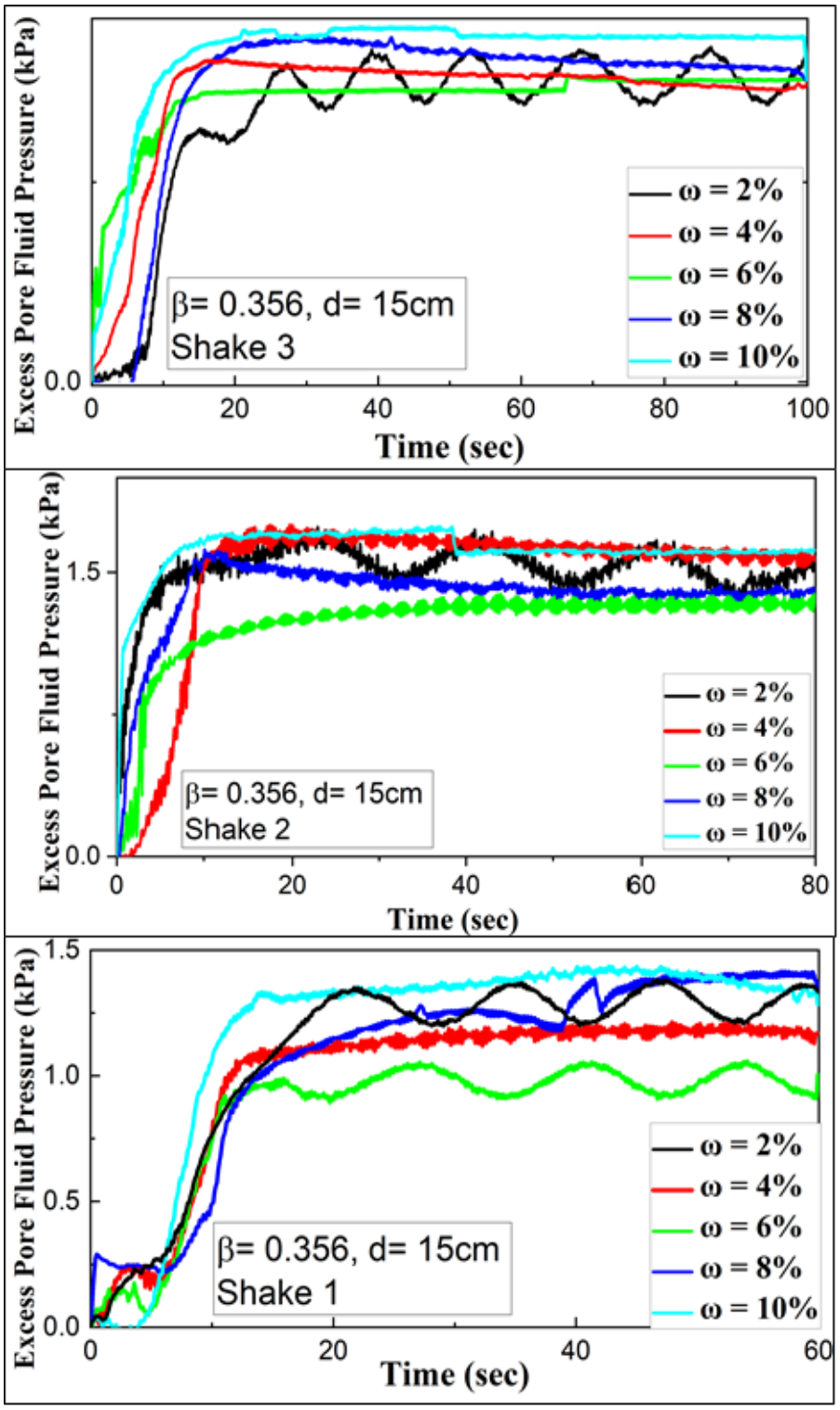


**Fig. 5.24 Excess pore pressure-time histories for different shaking events at varying oil content, ω, and β = 0.356 and d= 15**cm

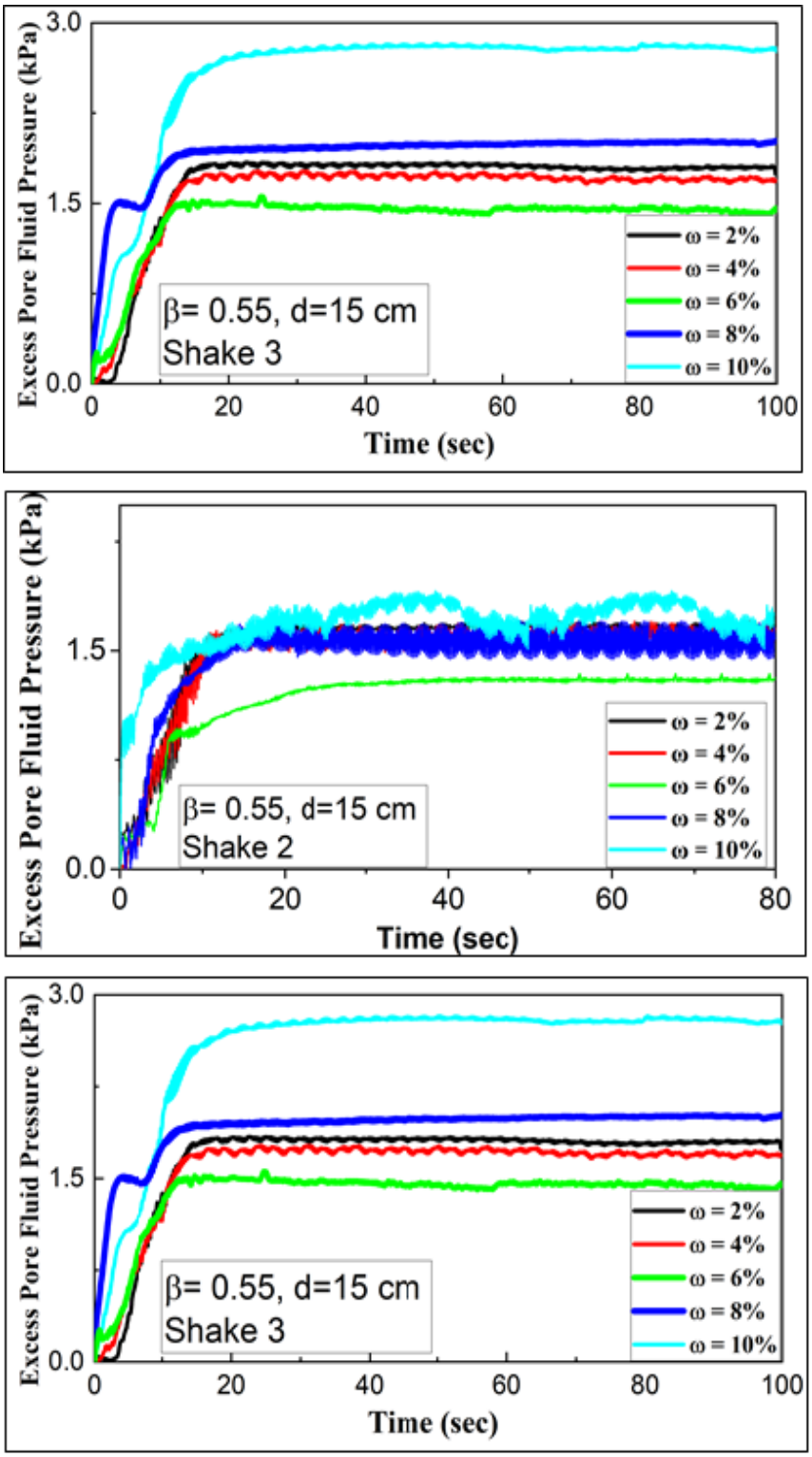


**Fig. 5.25 Excess pore pressure-time histories for different shaking events at varying oil content, ω, and β = 0.55 at 15 cm depth**

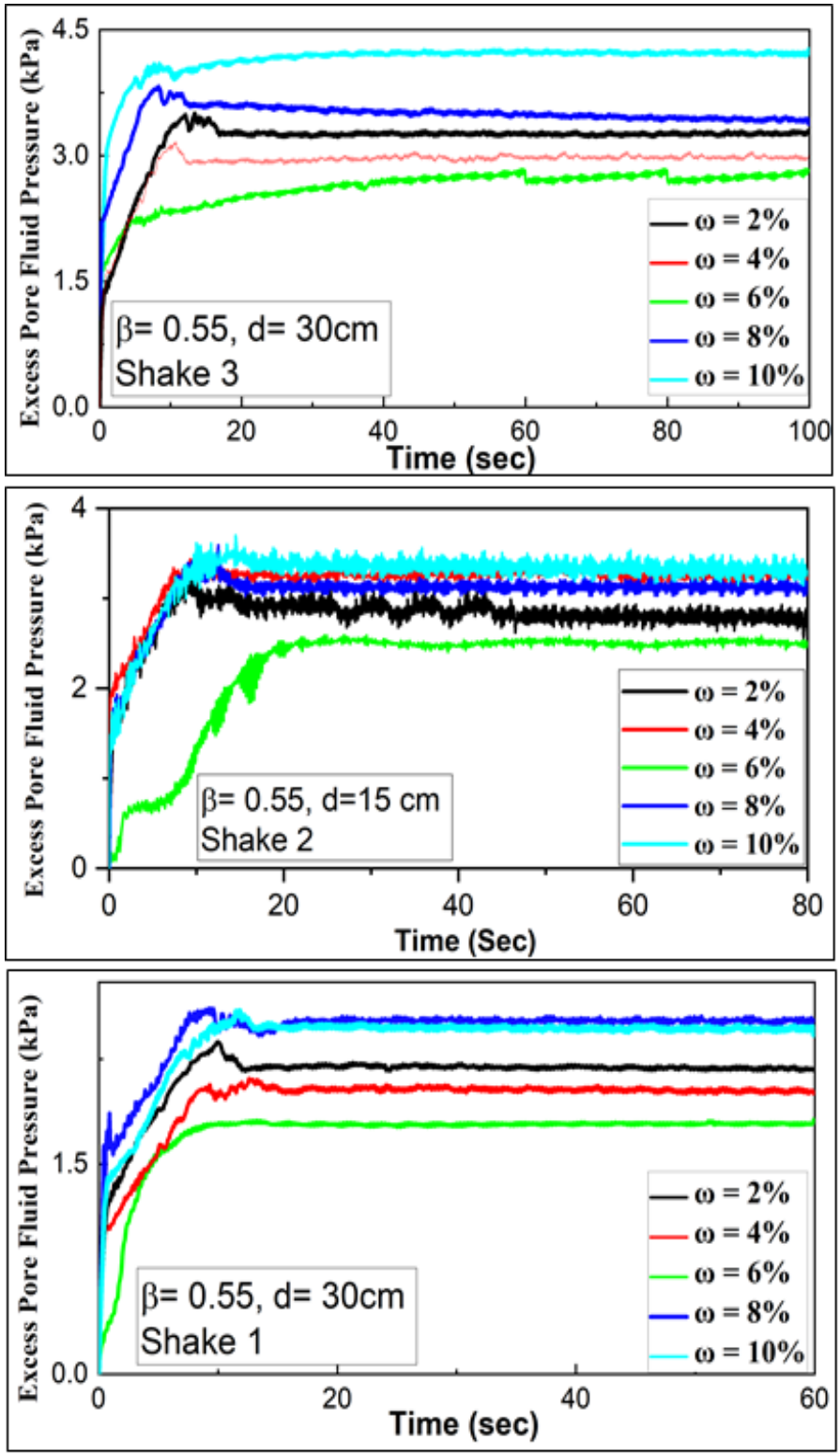


**Fig. 5.26 Excess pore pressure-time histories for different shaking events at varying oil content, ω, for β = 0.55 and d = 30 cm**

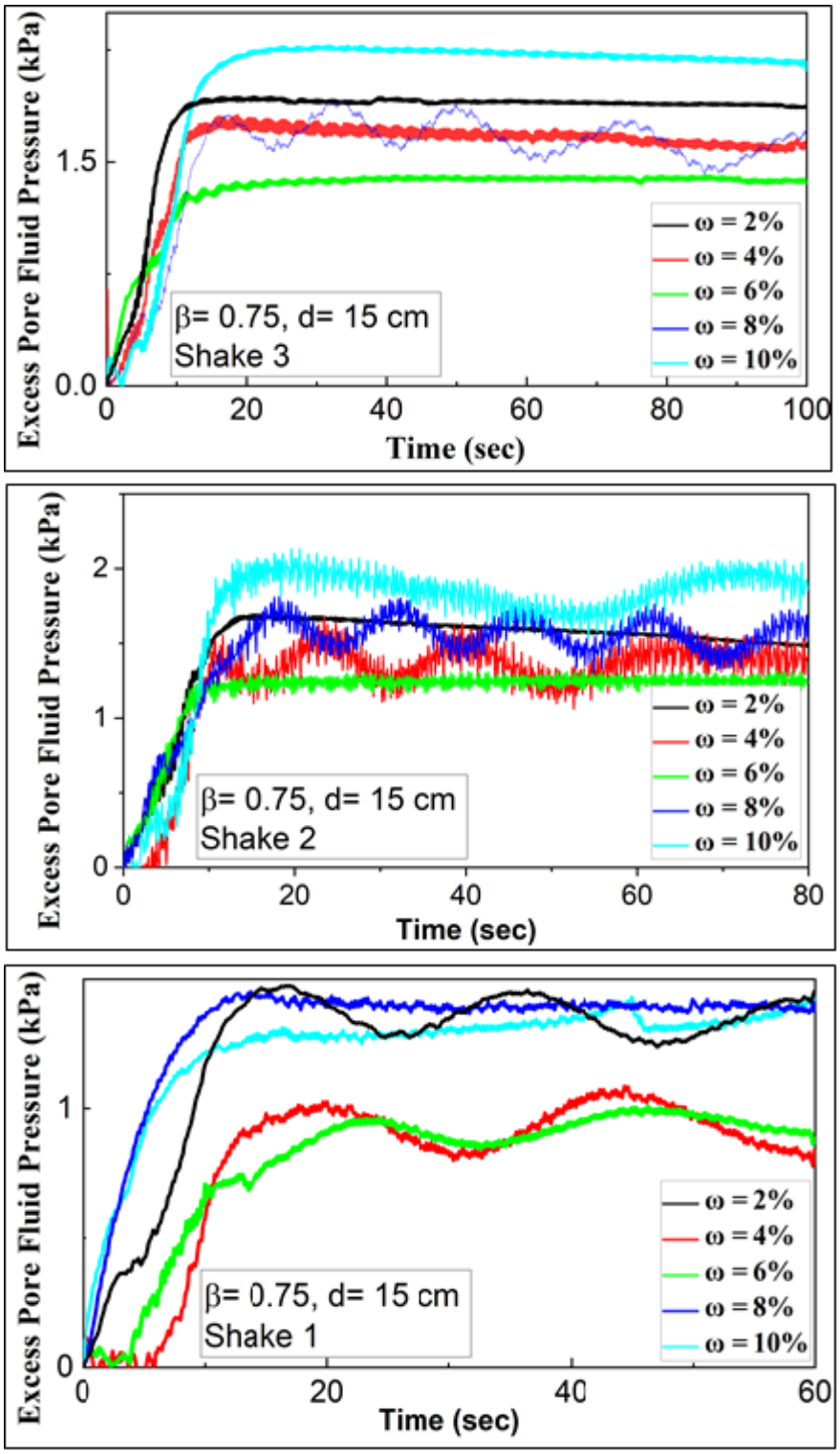


**Fig. 5.27 Excess pore pressure-time histories for first and third shaking events at varying oil content, ω, for β = 0.75 and d = 15cm**

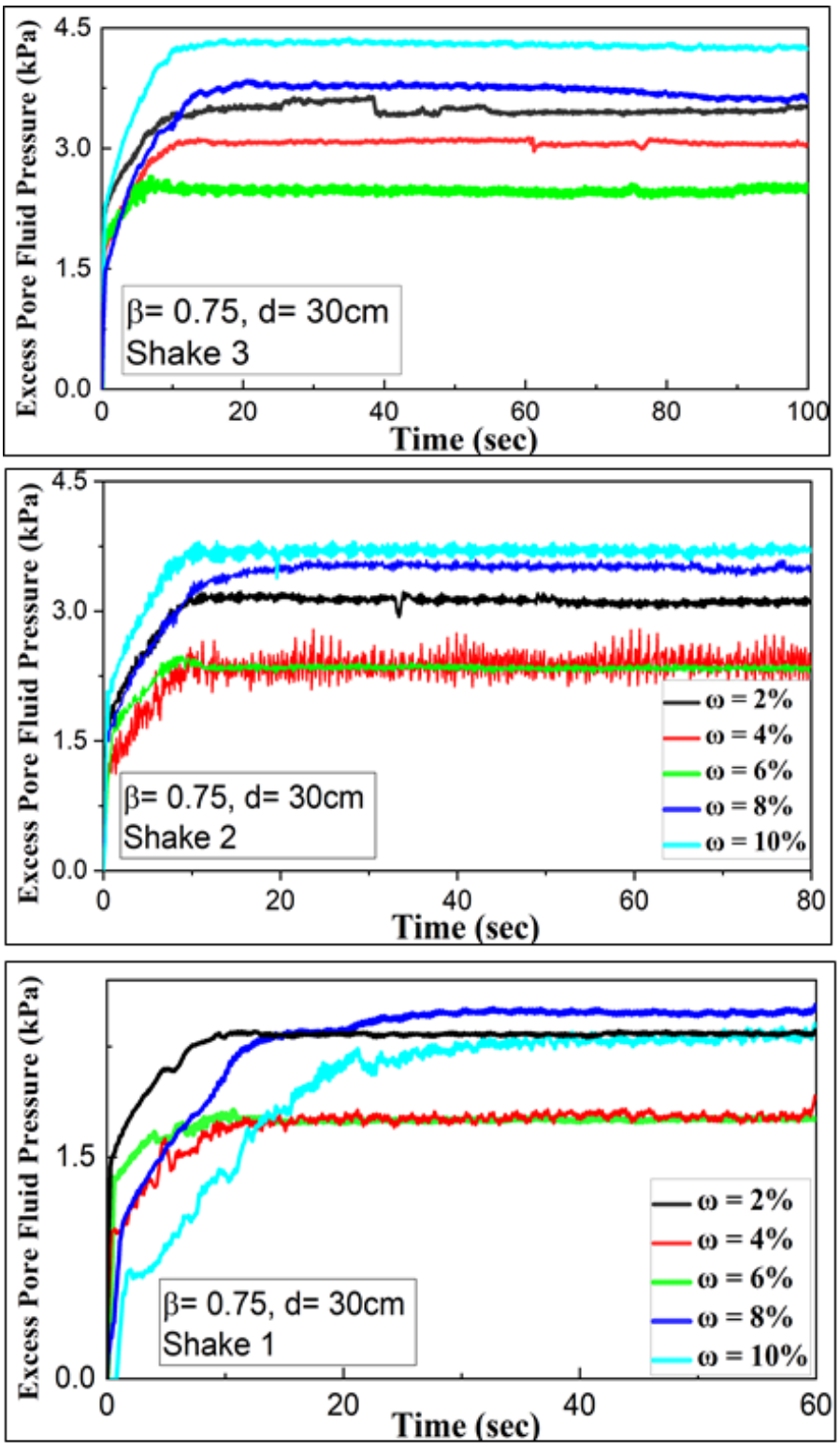


**Fig. 5.28 Excess pore pressure-time histories for first and third shaking events at varying oil content, ω, for β = 0.75 and d = 30cm**

In case of layered sand, the estimation of normalized pore pressure ratio was not as direct as in the case of homogeneous sand bed, since two layers were present at different bulk densities, while their relative densities were same. In such a case, average differential settlement of individual layers were recorded. The effective overburden stresses after shake 2 and shake 3 were calculated on the basis of the settlement of the individual layers. The selection of β ratio was such that the position of one of the pressure transducer lies at the interface of the contaminated and uncontaminated layer. The pore pressure ratio was then calculated by normalizing it with respect to effective overburden pressure. A comparison chart showing the maximum normalized pore pressure ratio and time for liquefaction initiation (if observed) under the three shaking levels for various values of ω and β at d = 30 cm. is shown in Fig. 5.29. Again, ω = 0% signifies homogeneous sand bed. The time taken for onset of liquefaction, $T_{L,}$ when $r_{u,max} \approx 0.88$ has been indicated against the respective oil content. It can be seen from the figure that in the event of first shaking, $r_{u,max}$ observed at ω = 2% was 0.91, 0.88 and 0.86 for β= 0.356, β= 0.55 and β = 0.75 respectively while at ω = 6% these values were 0.74, 0.62 and 0.59. With further increase in ω upto 10%, $r_{u,max}$ also increased to unity for each β value. Apart from that, the time taken for initiating liquefaction at ω= 2% increases from 53 seconds for β =0.356 to 55.7 seconds for β=0.55 and 58 seconds β = 0.75. This suggests that liquefaction was delayed with increase in the depth of contamination when the amount of contamination was relatively low. At ω =4% and 6%, no signs of liquefaction were seen during the entire duration of shaking. At ω = 8%, $T_L$ was reduced from 45.7 sec for β = 0.356 to 30.8 sec and 20.5 sec for β= 0.55 and 0.75 respectively. Following this, a sharp reduction in $T_L$ from 32 seconds to 24 seconds and 21

seconds was recorded at ω = 10% when β was correspondingly increased from 0.356 to 0.55 and 0.75.

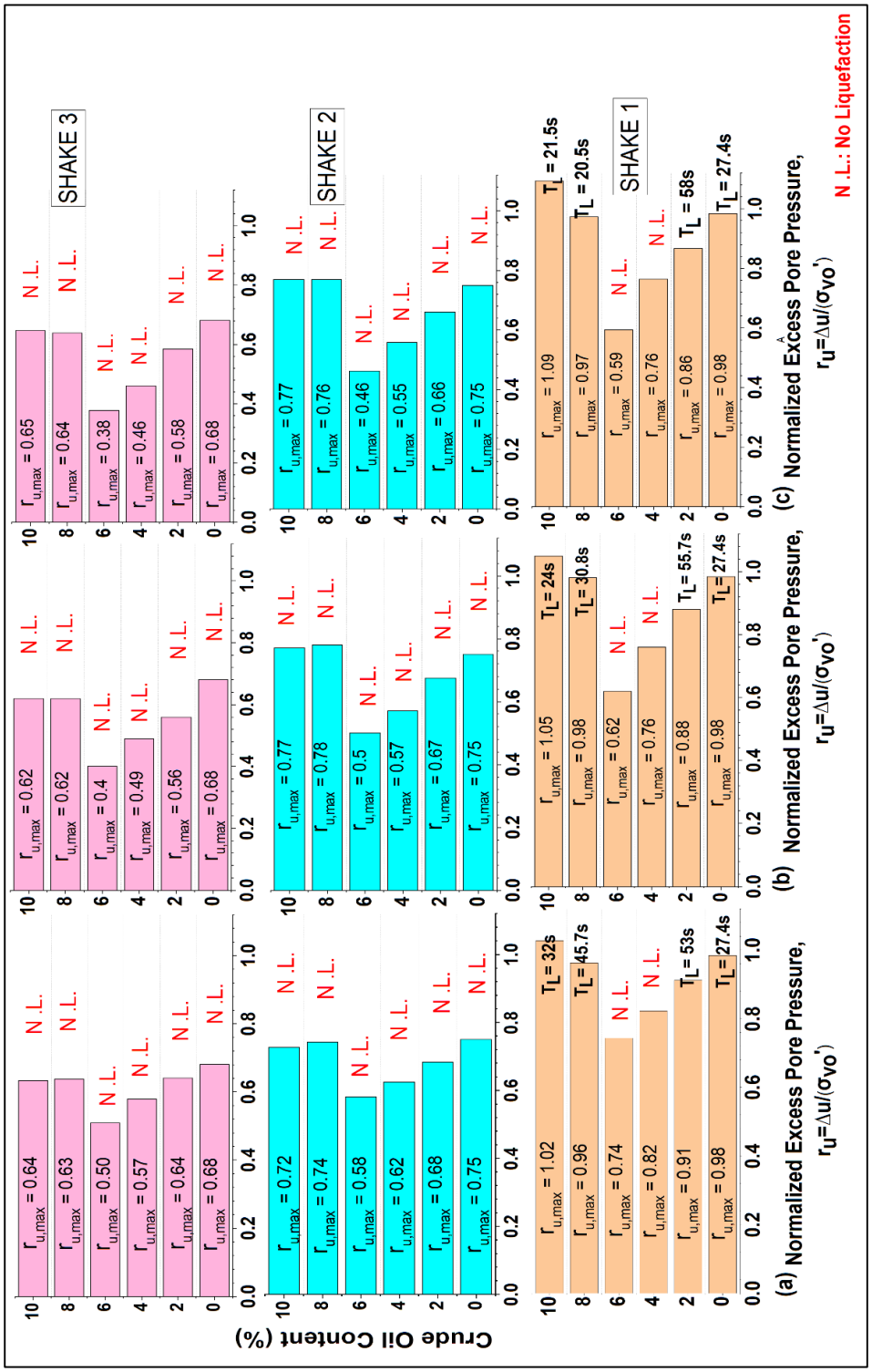


**Fig. 5.29 Comparison of maximum excess pore pressure ratio, $r_{u,\,max}$, and time to liquefaction, $T_L$ for homogenous sand bed at 30 cm depth for (a) β = 0.356, (b) β = 0.55, and (c) β =0.75**

*5.6.4 Coupled effect of Degree and Depth of Contamination*

Fig. 5.30 shows the coupled effect of the percentage of oil content and depth of contamination on the normalized pore pressure ratio. It is evident from the results explained in earlier sections that the crude oil contamination initially enhances the liquefaction potential upto a threshold point beyond which it showed diminishing effects. Likewise, it is also apparent from the figure that for a constant β ratio, increasing crude oil content brought a substantial reduction on liquefaction potential till the transition point corresponding to ω = 6% is reached. Adding further crude oil tends to increase the liquefaction susceptibility. The relationship between pore pressure ratio versus crude oil content results into a typical v-shaped profile with maximum resistance against liquefaction being offered at the trough. However, a remarkable damping was observed in the troughs of the $r_u$ profiles with decreasing β ratio indicating increase in $r_u$ and hence in liquefaction potential with decreasing β ratio.

It is important here to note that in case on first and second shaking events, there exists a value of ω (between 7.5% to 8%) at which the value of $r_{u,\,max}$ for contaminated samples were almost unchanged with respect to clean sand. This point was termed as *zero change point* in terms of liquefaction potential. Before this point, lowest liquefaction potential was observed for highest value of β. However, beyond this point, the variation of $r_{u,\,max}$ with β ratio gets reversed. For highest value β, highest liquefaction potential was observed. No evidence of such a point was observed after subjecting the sand bed to two subsequent shaking events.

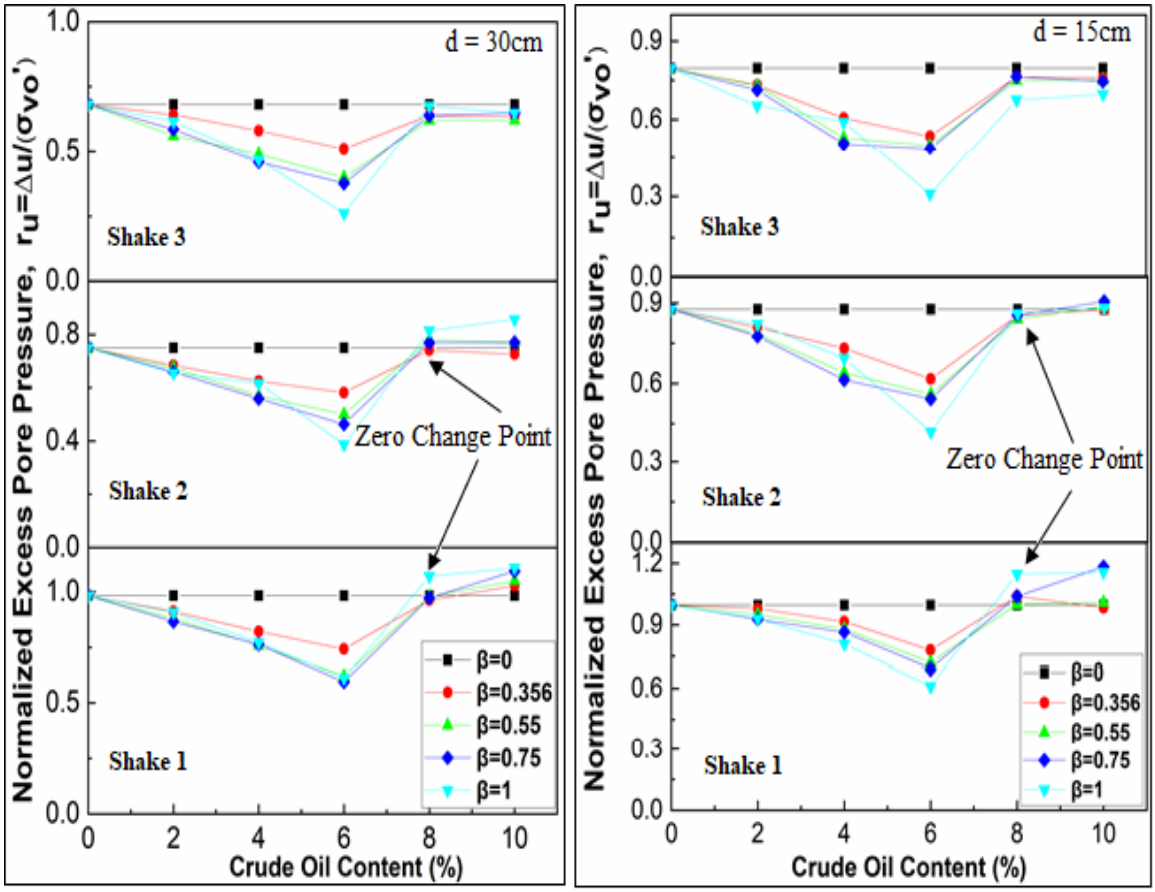


**Fig. 5.30 Coupled effect of variation in crude oil content, ω, and contamination depth ratio, β on normalized excess pore pressure ratio**

### 5.7 Summary

1-g model system is presented in this chapter in order to evaluate the effect of presence of hydrocarbon compounds on the liquefaction potential of Guwahati sand. The effect was extensively evaluated for different crude oil percentages, contamination depth ratio and shaking events. The observed test results can be summarized as follows:

- Initial contamination of crude oil moderately increases the liquefaction resistance up to ω = 6% after which it drops dramatically with further increase in crude oil up to ω = 10%. It was observed that $r_{u,\ max\ (\omega=0\%)} = 0.62 r_{u,\ max\ (\omega=6\%)}$ while $r_{u,\ max\ (\omega=0\%)} = 1.12 r_{u,\ max\ (\omega=10\%)}$ for the first shaking event.

- $\omega$ = 6% was considered as the threshold point below which the effect of crude oil was positive and beyond which the effect was deteriorating in concern with liquefaction resistance.
- Relatively higher resistance was observed during second and third shaking, particularly in contaminated sands, owing to higher degree of densification achieved due to lubricating effect of oil. The effect of oil contamination was reduced after first shaking as oil being lighter gets displaced from the pore spaces by the water.
- A zero change point exists at which the value of $r_{u,\,max}$ for contaminated samples were almost unchanged with respect to clean sand. The coupled effect of crude oil content and contamination depth ratio revealed a significant attenuation in the threshold point with increasing $\beta$ ratio before zero change point while a reverse trend was observed beyond this point.